Neutron Backgrounds in the Ricochet Experiment
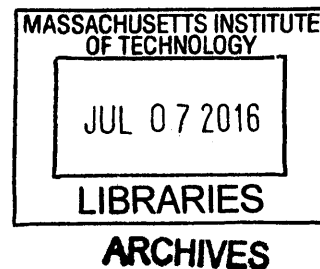
by

Elise Newman

Submitted to the Department of Physics
in partial fulfillment of the requirements for the degree of

Bachelor of Science in Physics

at the

MASSACHUSETTS INSTITUTE OF TECHNOLOGY

June 2016

Author .... **Signature redacted** ...

Department of Physics
May 6, 2016

Signature redacted

Certified by...
Joseph A. Formaggio
Associate Professor of Physics
Thesis Supervisor

Accepted by........ **Signature redacted** ...

Nergis Mavalvala
Chairman, Department Committee on Undergraduate Theses

Neutron Backgrounds in the Ricochet Experiment

by

Elise Newman

Abstract

This paper explores the impact of neutron backgrounds on the Ricochet experiment. The purpose of the Ricochet experiment is to determine the existence of sterile neutrinos via coherent neutrino-nucleus scattering. Coherent neutrino-nucleus scattering is an ideal detection method because it is a neutral current process. All active neutrino flavors will therefore be detected uniformly (no non-active, or sterile neutrinos will be detected because they do not couple to the Z boson). By varying the distance between the detector and the neutrino source, we consider deficits in neutrino flux to be evidence of oscillation to a fourth, non-active neutrino. Neutron backgrounds could interfere with neutrino detection. We therefore calibrate and employ Neutral Current Detectors (NCD's) for the purpose of neutron detection to measure the expected neutron spectrum incident on the detector. We furthermore design a Monte Carlo simulation to model the expected neutron capture rate of the neutrino detector in this setup.

Thesis Supervisor: Joseph A. Formaggio
Title: Associate Professor of Physics

Acknowledgments

Many thanks to Joseph Formaggio, Alexander Leder, and the rest of the Ricochet team for their guidance on this project! None of this would have been possible without their vision.

I am incredibly grateful for my undergraduate education in Physics at MIT. Through my professors and peers, I have learned so much these past four years, not just about physics, but also about learning, teaching, and scientific methods in general. This has been invaluable knowledge for me as it has helped me shape my life and my future meaningfully. I will be taking a break from physics to pursue a PhD in linguistics, but I very much hope to stay present in the physics community!

Special thanks to my mom for (besides making everything possible for me) teaching me how to think critically about my own learning process and how to approach problems with perspective.

Contents

List of Figures

List of Tables

Chapter 1

Introduction

Since the discovery of the neutrino, the picture of neutrino physics has proven to be increasingly complex. Until fairly recently, it was postulated that there were three massless neutrinos each corresponding to interactions involving electrons, muons, and tau particles respectively. Neutrinos were thought to be produced to have a specific 'flavor' (electron, muon, or tau) based on the decay of their corresponding charged leptons. However, there was a longstanding puzzle about electron neutrino flux from the Sun, namely that only a third of the predicted number was measured. This problem was referred to as the Solar Neutrino Problem[1]. Since a solution was found to the solar neutrino problem, it is now universally acknowledged that neutrinos oscillate between flavors, and therefore have nonzero mass [6]. The precision of neutrino detection experiments has steadily improved since this discovery, resulting in finer measurements of the relevant mixing and mass parameters.

Despite the remarkable success of the neutrino oscillation picture, discrepancies between these measurements and theoretical predictions has revealed increasing complexity in the standard picture of particle physics. Several experiments have measured a $\sim 3\sigma$ [8] deviation from theoretical predictions that may either be the result of 1) difficult to predict effects on the experiment or 2) the existence of new physics. One proposal involves the introduction of a fourth neutrino flavor, a sterile neutrino that

---

[1]Many experiments measured this discrepancy: Brookhaven National Laboratory (measured solar neutrinos) and SuperKamiokande in Japan (measured solar and atmospheric neutrinos) to name a few. See Appendix B for more details.

is not predicted by the standard model.

The Ricochet experiment proposes use of the well predicted process of coherent elastic neutrino-nucleus scattering to probe sterile neutrino oscillations. As coherent neutrino-nucleus scattering has not yet been observed, it is our goal to first measure this process using the MIT Research Reactor as a neutrino source. Coherent neutrino scattering has the experimental signature of a nuclear recoil. We measure the recoil energy due to scattering with a cryogenic crystal bolometer made of a semiconductor metal (osmium in this case). We will furthermore test whether using superconducting metals could deliver phonon-only sensitivity to remove backgrounds due to electromagnetic interactions.

If we succeed in measuring coherent neutrino scattering, we plan to look for the sterile neutrino signature using an intense source. At low enough energies, the signature of oscillation from active to sterile neutrinos is on the order of meters [5]. We can therefore easily vary the distance between the osmium detector and the source in order to measure relevant deficits in active neutrino flux, implying oscillation to sterile neutrinos. The shortcoming of such a method for neutrino detection is that it may be difficult to distinguish neutrino events from various backgrounds, neutron radiation in particular. To circumvent this problem, we include calibrated Helium 3 proportional counters in the experimental setup for the purpose of neutron detection. The Helium 3 detectors were calibrated using a dedicated neutron source as well as an americium-beryllium source at the MIT Research Reactor. Using the neutron spectrum measured at the reactor with the calibrated neutron detectors, we designed a Monte Carlo simulation using Geant4 to predict the event rates on the osmium crystal due to neutrons from the reactor itself.

This paper focuses on neutron backgrounds. It provides a detailed account of the calibration process for the Helium 3 proportional counters, as well as the results of the Monte Carlo simulation.

Chapter 2

Sterile Neutrinos and Neutrino Coherent Scattering

2.1 Sterile Neutrinos

In 1930, Pauli proposed the existence of a light, neutral particle to account for missing kinetic energy in nuclear beta decay. In nuclear beta decay, some element A is transformed into a lighter element B via emission of an electron,

$$\,^{N}_{Z}A \longrightarrow \,^{N}_{Z+1}B + e^-. \tag{2.1}$$

The electron was predicted to have fixed energy based on the rest mass and momentum of each element. However, experiments measured highly variable kinetic energy for the electron. The options were to either abandon energy conservation, or adopt the existence of an unseen particle to carry away the extra energy. The latter proposal was more widely accepted and this particle was called a *neutrino*. Three different types of neutrinos were predicted, and later measured; electron, muon, and tau neutrinos. Each of these flavors corresponds to the lepton (electron, muon, or tau) produced in nuclear decay. [10]

It was later shown as a solution to the solar neutrino problem that these three neutrinos oscillate between flavors via a mixing matrix. We say neutrinos 'oscillate'

to mean that the probability of measuring a neutrino of a specific lepton flavor oscillates as the neutrino propagates through space. We can write the different neutrino flavors as different superposition states (generally called flavor states) of a common underlying basis (generally called mass states). For example, if we take a two-state system of electron and muon neutrinos, the mass basis is $\{|\nu_1\rangle, |\nu_2\rangle\}$, and the flavor basis is $\{|\nu_e\rangle, |\nu_\mu\rangle\}$. They transform via the following matrix,

$$\begin{pmatrix} |\nu_e\rangle \\ |\nu_\mu\rangle \end{pmatrix} = \begin{pmatrix} \cos\theta & \sin\theta \\ -\sin\theta & \cos\theta \end{pmatrix} \begin{pmatrix} |\nu_1\rangle \\ |\nu_2\rangle \end{pmatrix}. \tag{2.2}$$

In this system, the probability of measuring an electron neutrino at some propagation distance L is,

$$P_{\nu_e}(L) = \sin^2(2\theta)\sin^2\left(\frac{c^3 \Delta m^2 L}{4\hbar E}\right), {}^1 \tag{2.3}$$

where Δm^2 is the mass difference between electron and muon neutrinos, θ is the mixing parameter, and E is the neutrino energy. Since the proposal of neutrino oscillation, it has been the goal of many experiments to measure the mixing and mass parameters governing this oscillation.

Recently, observations at LSND, MiniBooNE, and reanalysis of reactor data measured oscillation signatures with a significant discrepancy in mixing parameters compared to earlier experiments [8]. A likely novel explanation for these results is the existence of a fourth neutrino with a mass scale of ~ 1 eV [1]. The need for this novel explanation is ambiguous because other experiments, such as CDHSW and MINOS, measured no such discrepancies. Despite this ambiguity across experiments, the uniformity of the results among LSND, MiniBooNE, and others is interesting and worth investigation. They have all shown a Δm^2 that is $\sim 3\sigma$ greater than the largest mass splitting difference both predicted and verified through prior measurements.

Results from CERN show that if there is a fourth neutrino flavor, it cannot couple with the Z boson, and thus should be called 'sterile', while the other three neutrino flavors are called 'active'. Further experiments will hopefully determine if the data

---

[1]For a full derivation, see Appendix B.

consistently diverge from standard model predictions, thus determining the need for this novel explanation. In the meantime, the Ricochet experiment addresses the question of the existence of a non-active, or sterile neutrino, by making use of neutrino-nucleon coherent scattering.

Coherent scattering is an advantageous approach for detecting the signature of sterile neutrinos for several reasons. First, it is a neutral current process. Neutral current couples to all active neutrino species, regardless of flavor. Therefore, an observed oscillation is evidence for the existence of sterile neutrinos, as oscillations between active flavors would not be noticed if all active neutrinos are measured without distinction. Furthermore, active neutrinos will scatter off nuclei uniformly without differentiating between protons and neutrons, thus amplifying the cross section significantly. Because it is predicted that sterile neutrinos should not interact at all, our measurements of them will be based off the following mixing probability distribution [8],

$$P(E_\nu, r) = 1 - \sin^2\left(2\theta_S\right)\sin^2\left(1.27\Delta m_S^2 \frac{r}{E_\nu}\right), \tag{2.4}$$

where $\sin^2\left(2\theta_S\right)$ is the oscillation amplitude, Δm_S^2 is the sterile mass splitting in eV^2, E_ν is the neutrino energy in MeV, and r is the distance from the detector measured in meters. At sufficiently low energies, the length scale r is on the order of meters. Therefore, as we vary the distance between the neutrino source and detector, decreases in flux will signify oscillation to sterile neutrinos. Low energy detection is therefore crucial to easily measuring the signature of sterile neutrinos.

An advantage of using metallic superconducting targets for this technique is that any charged current interaction will produce quasi particles while neutral current interactions with the crystal lattice will only impart kinetic energy, producing phonons. This provides an ideal opportunity for filtering out the signal of charged backgrounds.

2.2 Coherent Scattering

Coherent neutrino-nucleon scattering was predicted about 30 years ago by Daniel Freedman [9]. It is a quantum mechanical phenomenon that is an ideal detection method because of the way in which the nucleus' cross section is amplified. For a neutral current process, the neutrons and protons become indistinguishable to an incident neutrino such that their cross sections add coherently.

The theory of coherent neutrino-nucleon scattering is best understood in relation to the difference between neutral current and charged current processes. We refer to charged current as the following process [10],

$$W^+$$

$$\nu_l \qquad \qquad l^-$$
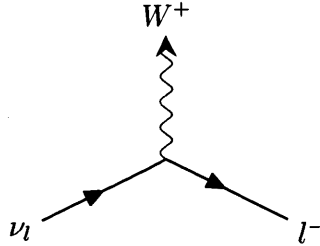
Figure 2-1: A diagram outlining charged current processes.

where ν_l is a neutrino corresponding to some lepton l. Here, some neutrino is converted into its corresponding lepton via emission of a W^+ (or absorption of a W^-). Charged current processes are mediated by the W bosons while neutral current processes are mediated by the Z boson.

$$Z$$

$$f \qquad \qquad f$$
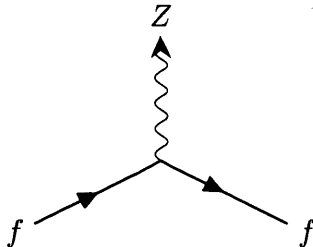
Figure 2-2: A diagram outlining neutral current processes.

Neutral current processes refer to interactions where some fermion scatters off a target and is emitted as the same fermion, emitting a Z boson in the process. In the

case of neutrino-nucleon coherent scattering, this refers to a neutrino scattering off a nucleon, releasing another neutrino. This process is shown below in figure 2-3, where N refers to some nucleon, either a proton or a neutron.
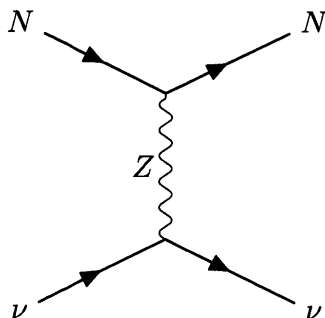
Figure 2-3: A diagram outlining neutrino-nucleon scattering.

This is considered to be a coherent process because neutral current processes involving a neutrino will release another neutrino regardless of what the interacting nucleon is. This insensitivity to whether the neutrino scatters off of a neutron or a proton increases the cross section of a nucleus by adding the cross section of each nucleon coherently. It should be noted that since sterile neutrinos do not couple to the Z boson, sterile neutrinos can never participate in a neutral current process. Using coherent neutrino-nucleon scattering as a detection mechanism allows us to measure only active neutrino fluxes. We measure sterile neutrinos indirectly by varying the propagation distance of the neutrinos. Based on the aforementioned probability distribution, we consider deficits in active neutrino flux to be evidence of oscillation to sterile neutrinos.

The coherent scattering cross section σ of an incoming neutrino with energy E_ν is [5] [9],

$$\frac{d\sigma}{dT} = \frac{G_F^2}{4\pi} Q_W^2 M \left(1 - \frac{MT}{2E_\nu^2}\right) F(q^2)^2, \tag{2.5}$$

where T is the recoil energy, M is the mass of the target, $F(q^2)$ is the nuclear form factor and G_F and Q_W are the Fermi constant and weak charge respectively. The weak charge is defined,

$$Q_W = N - (1 - 4\sin{\theta_W}^2)Z, \qquad (2.6)$$

where N is the number of neutrons and Z is the number of protons in the target material. This experiment mainly considers monoenergetic electron-capture sources with neutrino energies below 1 MeV. The recoil energies predicted for neutrino-nucleon coherent scattering are extremely low, accounting for the absence of experiments employing this technique. The maximum kinetic energy imparted on the nuclear recoil is

$$T_{max} \leq \frac{E_\nu}{1 + \frac{M_A}{2E_\nu}}, \qquad (2.7)$$

where M_A is the mass of the recoil target and E_ν is again the neutrino energy.

To achieve an oscillation signature on the order of a few meters, we use a neutrino source that produces neutrinos at approximately 1 MeV. For a silicon target (mass of approx. $26\,\text{GeV}/\text{c}^2$), the maximum recoil energy is approximately 50 eV, necessitating a threshold energy of about 10 eV. For an osmium target, which has a mass of about $180\,\text{GeV}/\text{c}^2$, the maximum recoil energy is even lower (approx. 15 eV). It is very difficult to achieve threshold energies this low. However, low temperature bolometers, which are frequently used for dark matter detection, can achieve this low threshold energy [8].

2.3   The Complete Detection Mechanism

The experimental setup involves a semiconductor metal in a crystal array, which functions as a bolometer, cooled in an Adiabatic Demagnetization Refrigerator (ADR). The ADR we use is a Cryostat Model 103 Rainier, which has a base temperature of 50 mK. More detailed information about the ADR can be found in Appendix A.

The energy threshold for a bolometer depends on its baseline energy resolution, which in turn, depends on its temperature, resistance, and heat capacity. By cooling the crystal, we ensure a conduction path from the bolometer to a cold bath. An

extremely low heat capacity is required to achieve a low enough threshold energy. As heat capacity is roughly proportional to temperature cubed, a low temperature is also required to achieve a low enough heat capacity, which in turn lowers the threshold energy. [4]

By cooling the crystal, we also provide a mechanism for filtering out the signal due to charged backgrounds. When a semiconductor is cooled sufficiently, it super-conducts. Any quasi-particles created by charged current interactions will take much longer to reach thermal equilibrium than they normally do. Due to their increased lifetimes, the resulting signal will be a long tail as opposed to a sharp peak. These long tails will be nearly indistinguishable from thermal noise, thus allowing us to isolate the well-defined signal due to neutral current interactions.
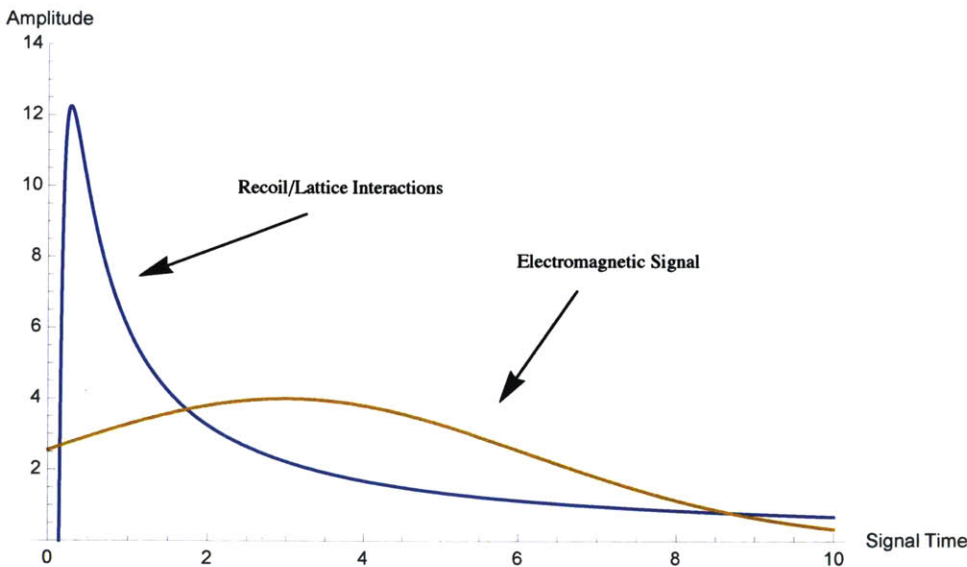
Figure 2-4: The difference in neutral/charged current signals due to the superconducting crystal.

The setup will take place at the MIT Research Reactor (MITR), which will act as a strong source of neutrinos with energies of a few MeV. The neutrinos from the reactor will impart kinetic energy on the crystal lattice, creating phonons. These phonons will be converted to quasi particles to create an electric signal.

Neutrons are also produced in the fission process that powers the reactor. As neutrons will interact similarly with the detector, helium 3 proportional counters will

be included in the setup to help determine how many neutrons there are in the system, and thus filter out those events from the neutrino measurements.

Chapter 3

Neutral Current Detectors

Neutrons also induce a recoil in our detecter, and therefore have the same experimental signature as neutrinos. Since neutrons are also produced at the nuclear reactor, and in a similar energy range to the neutrinos, it is likely that our osmium detector will measure a significant number of neutron events as well. It is therefore important that we first determine the neutron spectrum present in the environment for our experimental setup. To do this we use a helium 3 proportional counter as a neutron detector, or neutral current detector (NCD).

3.1   The NCD

Helium 3 proportional counters are a well-established method for neutron detection due to helium 3's enhanced cross section for neutrons[1]. Gas proportional counters generally consist of a tube of gas with a central anode wire. The cylinder is grounded while high voltage is applied to the anode wire, thus creating a strong electric field radially about the wire. The wire's diameter is generally very small, on the order of 10's to 100's of microns, meaning that the electric field close to the wire's surface is very high ($\sim 10^6 - 10^7$ N/C). Free electrons therefore move almost exactly radially inward. [11]

---

[1]Helium 4 is also known for it's ideal cross section for neutrons. However, helium 4 is ideal for high energy neutrons while helium 3 better captures thermal neutrons. This is a low energy experiment in which we are only concerned with thermal neutron backgrounds.

Incoming particles collide with gas atoms, ionizing them and creating electron-ion pairs, which drift towards the central anode wire. These electrons cause further ionization, eventually initiating an avalanche of electrons of order $10^2 - 10^5$ electrons, which is large enough to produce an electric signal. A high voltage supply is required so that even small cascades hitting the central wire will be distinguishable from noise. [11]

Incident neutrons undergo the following reaction inside our helium 3 proportional counters. [3]

$$^3He + n \rightarrow p + {}^3H + 764 \text{ keV}. \tag{3.1}$$

In this reaction, the proton carries away 573 keV of the energy and the triton carries 191 keV. These ions create a cascade of electron-ion pairs, which drift to a central anode wire. As stated above, avalanche multiplication results in large numbers of secondary electron-ion pairs that produce an electric signal.

The neutron spectrum of a helium 3 proportional counter is not exactly a sharp peak at 764 keV, but rather a spread across energies 191-764 keV with a maximum at 764 keV. Energy deposition lower that 764 keV is the result of protons or tritons striking the wall before stopping in the gas. Total absorption of the proton's energy in the wall results in 191 keV energy deposition. For energy depositions below 191 keV, both particles would have to hit the wall, which is incredibly unlikely due to limitations on the geometric phase space [3].

The NCD's used in the Ricochet experiment are from the original SNO experiment, and therefore have low levels of uranium and thorium contamination. This contamination gives rise to the main source of backgrounds, which are alpha particles produced by nuclei embedded in the walls. These alpha particles can cause ionization events in a large range of energies, including the region of interest for neutron captures. Other forms of backgrounds such as electrons from beta decays or Compton scattering have less of an effect because many iterations of multiple scattering are required before sufficient energy can be deposited from the process.
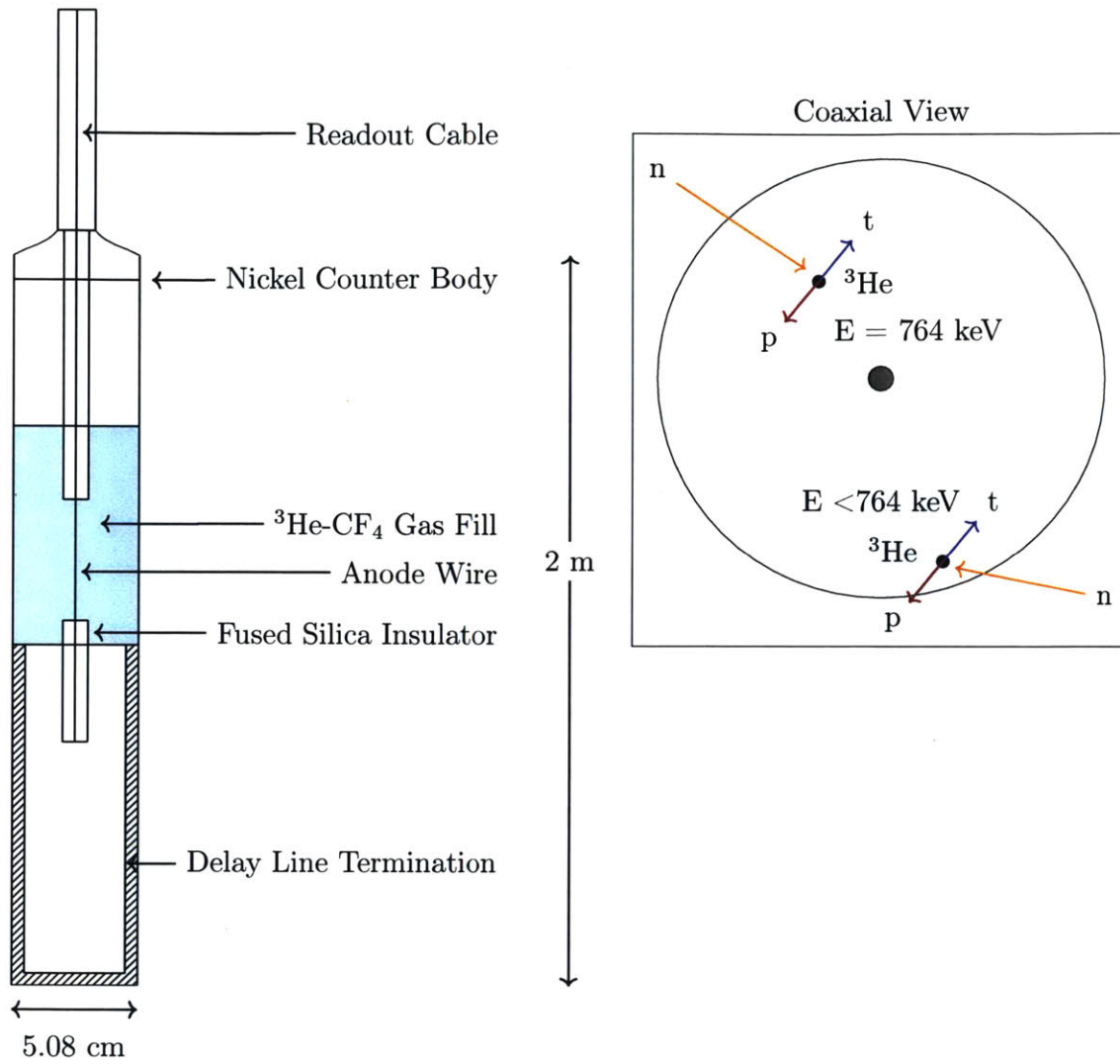
Figure 3-1: A diagram of the NCD including a coaxial view illustrating the process of neutron captures.

3.2 Calibration

The MITR is powered by fission of $^{235}_{92}U$, which produces (among other things) mostly thermal neutrons (as opposed to high energy neutrons). Some higher energy neutrons are created in the process but most of them are successfully 'cooled' to thermal energy levels such that they can contribute to the chain reaction of fission [7]. The neutron spectrum from the reactor incident on our experimental setup is not known. In order to measure it accurately, and thus more accurately measure the neutrino flux, we

calibrate the NCD's using a number of sources with known neutron spectra.

The first calibration source is a dedicated neutron source (DD source) that produces monoenergetic neutrons (a flat spectrum). This source is not included in our final setup. The next source is an americium-beryllium (AmBe) source that will be in the vicinity of our experiment. We took a number of measurements with each of these sources using degrees of shielding to build a spectrum. This paper focuses on the results of the DD source but not the AmBe source.
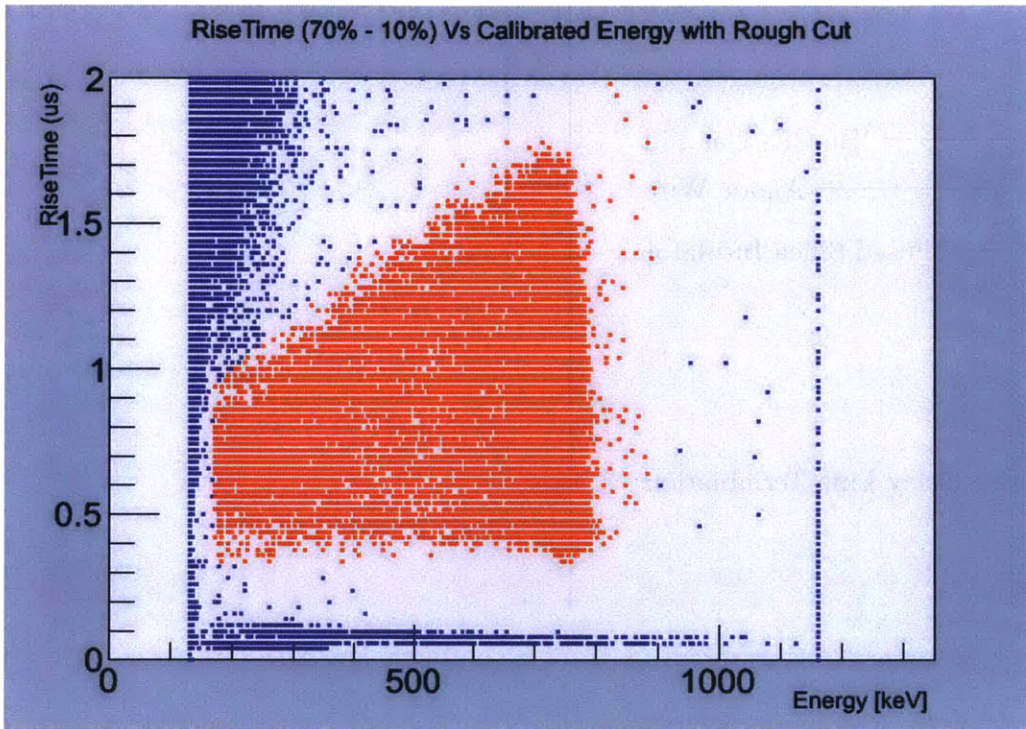
Figure 3-2: An example of a triangle plot used to isolate the thermal neutron captures in the NCD's.

As the NCD's pick up signals from different backgrounds as well as neutrons, we use pulse shape discrimination to isolate thermal neutrons. The above triangle plot shows energy deposited versus pulse rise time. Particles with high rise time and low energy are from low ionizing events (these are colored blue in figure 3-2). High energy particles are usually alpha particles and are also colored blue. The neutron recoils are localized to the red triangle because they have slower rise time. The rightmost edge of the triangle drops off sharply at around 764 keV due to the energy peak in

the reaction.
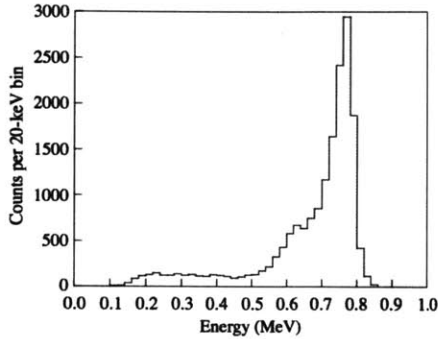
(a) The neutron energy spectrum measured by the NCD's [3].
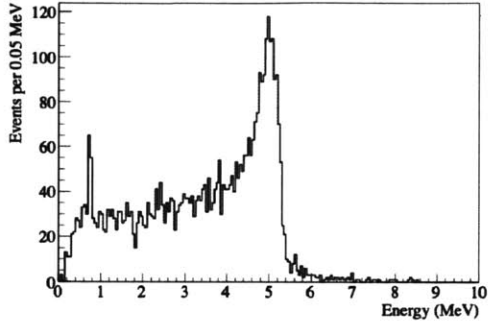
(b) The alpha energy spectrum measured by the NCD's [3].

Figure 3-3: NCD energy spectra for neutrons and alphas [3].

3.2.1 Shielding Layers

To measure the energy spectrum of the neutrons, we took a series of measurements involving 6 layers of shielding around the detector. As we increase the shielding around the detector, the threshold energy for a neutron to reach the detector increases (lower energy neutrons are impeded by the shielding). We therefore measure the neutron flux associated with each layer to better understand how many neutrons in each energy region are captured by the NCD, resulting in an energy spectrum.

The shielding layers are all made of PVC and fit together concentrically around the detector body (as seen in figure 3-4)[2]. Below are some triangle plots from DD source measurements, taken with various shielding layers to show that the energy peak shifts with the amount of layering. As the number of layers increases, the peak becomes narrower as fewer lower energy neutrons are captured.

---

[2]In reality, it is very difficult to cut PVC cylinders such that they all stack perfectly concentrically around the detector, while still maintaining ease of removal. Therefore, the actual setup involves the detector resting on the bottom of its closest cylinder, which likewise rests on the bottom of the next layer, etc. It is unlikely that this has a significant effect on our results.
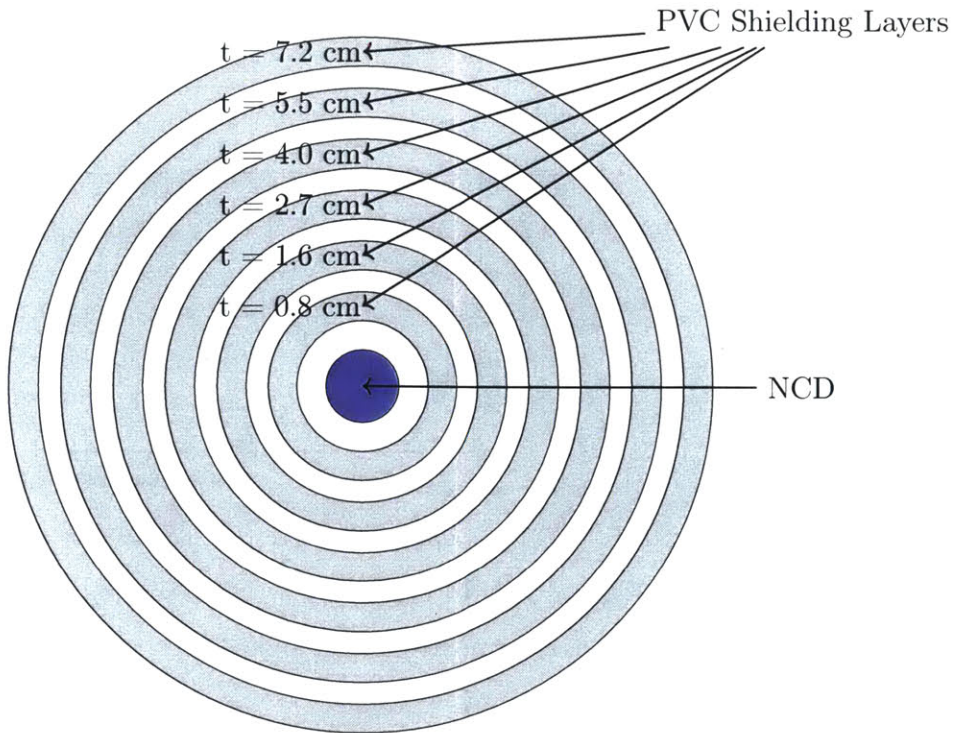
Figure 3-4: A cross-sectional view of the NCD surrounded by 6 concentric PVC layers with cumulative thickness t.
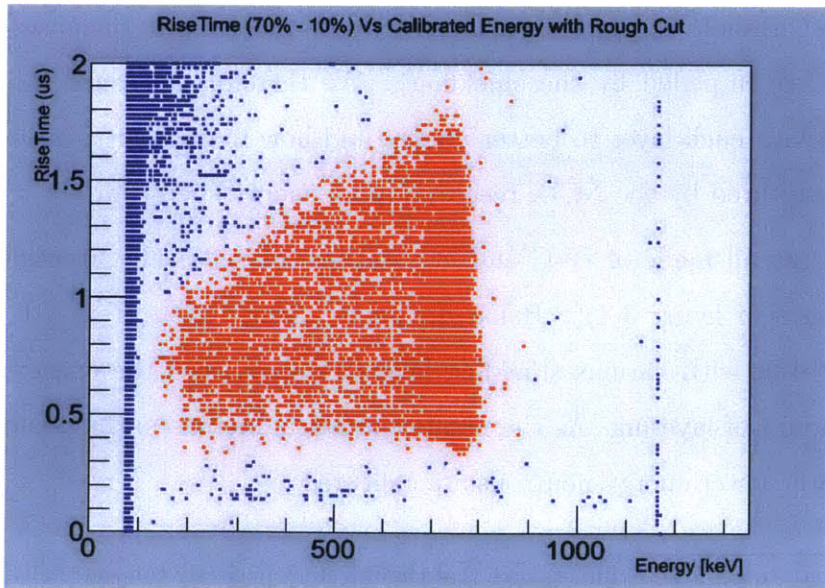

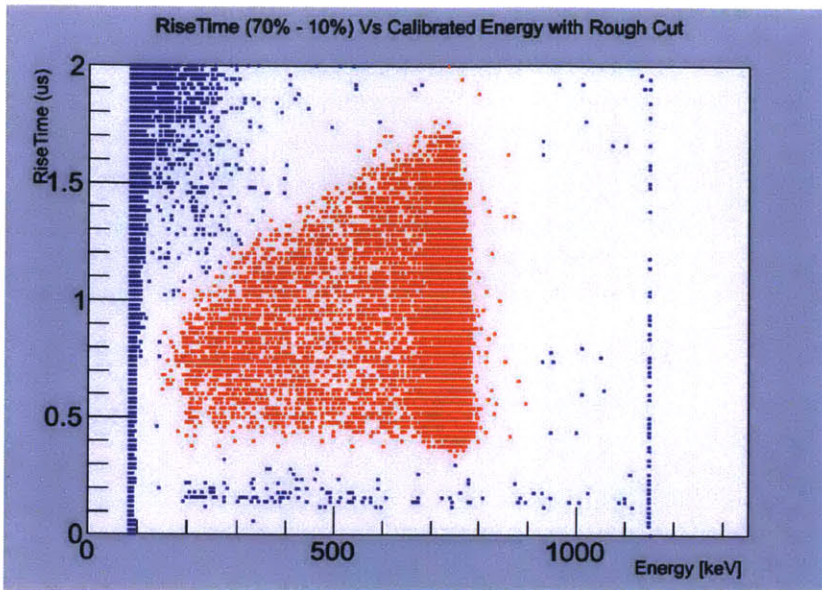Figure 3-5: Triangle plot showing 0 shielding layers.
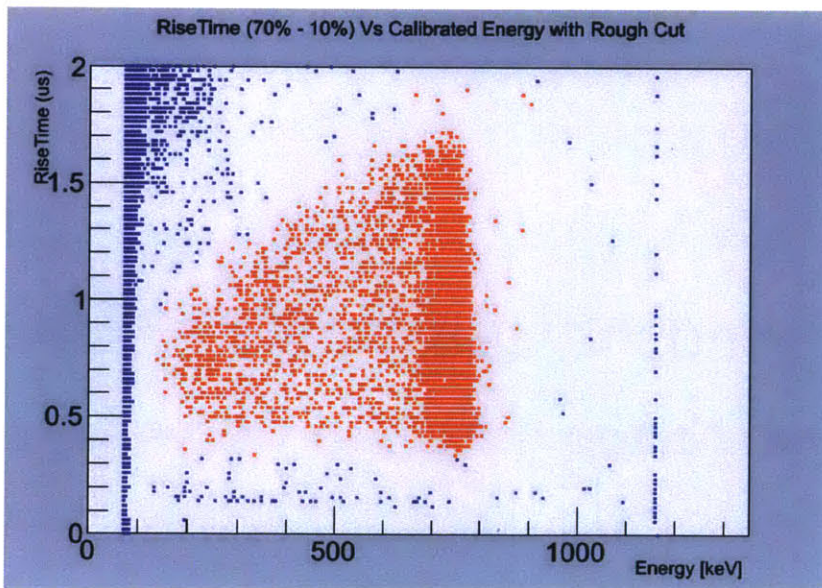
Figure 3-6: Triangle plot showing 1 shielding layer.

Figure 3-7: Triangle plot showing 2 shielding layers.

Chapter 4

The DD Source

NCD measurements were taken with a dedicated deuterium-deuterium (D-D) neutron source with a flat spectrum. These measurements were used to calibrate the NCD by analyzing 1) how effectively the NCD and PVC layer system captures this flat spectrum, and 2) what amount of shielding corresponded to which neutron energies.

The neutron source makes use of deuterium-deuterium collisions to create mono-energetic neutrons with a total kinetic energy of 2.2 MeV. The neutron source consists of a filament, a cathode, a grid, a collector, and a high voltage target. One end of the source is low voltage while the other end is high voltage. The filament has deuterium baked onto it. When the filament is set to 2 V and subjected to 2 Amps of current, it heats up and deuterium is released toward the cathode. The cathode is held at 4 V and 2.3 Amps and the grid is held at 200 V potential. There is therefore an electric field between the cathode and the grid. As the electrons accelerate from the cathode to the grid, the deuterium atoms occasionally collide with them and the deuterium atoms become ionized. These ionized deuterium atoms are collected and sent to a titanium target coated with deuterium. The target is held at a high voltage of 33 kV. The collisions between the deuterium atoms and the target create neutrons at 2.2 MeV and ^{3}He. Titanium is an ideal target material because it forms a stable compound with the deuterium surface layer. The deuterium-deuterium collisions produce neutrons by the following process.

$$^2H + {}^2H \longrightarrow {}^3He + n \qquad (E_n = 2.45 MeV) \qquad (4.1)$$
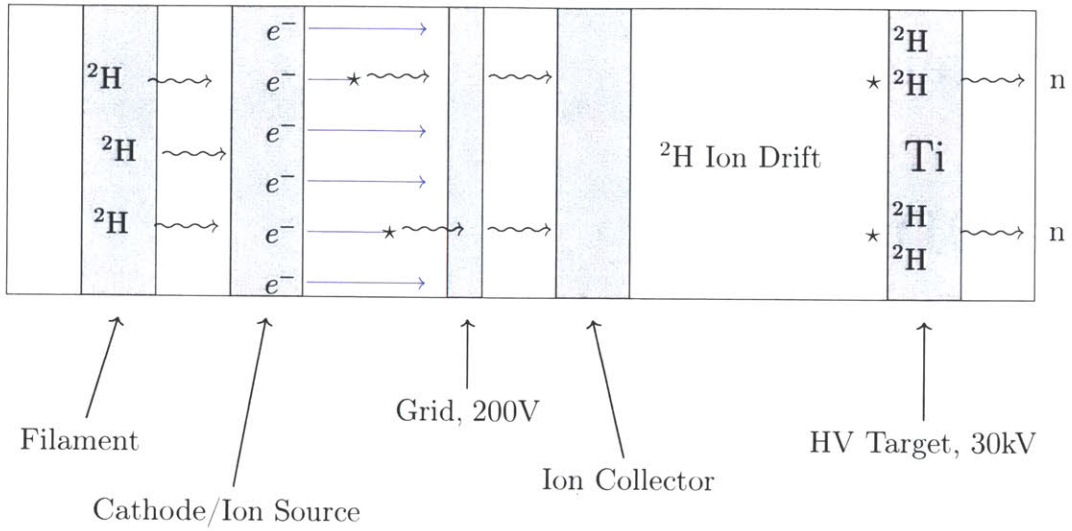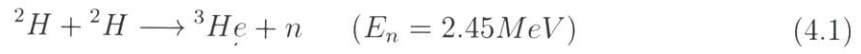
Figure 4-1: A schematic of neutron production in the source.
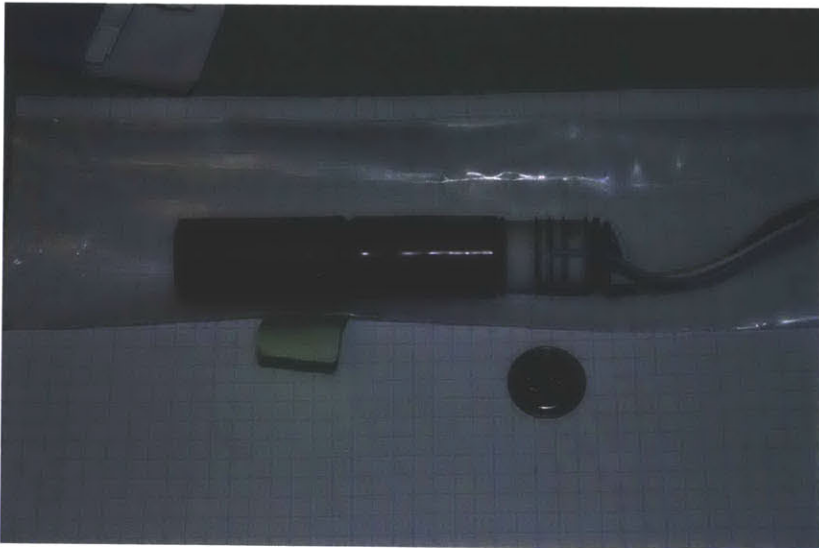
Figure 4-2: A picture of the neutron source with a quarter for scale.

As the source is subjected to very high voltage, the entire source is submersed

in a mineral oil bath. This prevents discharges or heat conduction to the case. A bonner sphere was also placed next to the detector to monitor neutron radiation in the surrounding area.

Measurements were taken at several distances from the source, with varying shielding layers, and varying voltages for the target.

Chapter 5

The Neutron Monte Carlo

We designed a Monte Carlo simulation using Geant4 [2] to model the proposed backgrounds incident on the experimental setup. By comparing this to measurements taken with the NCD's, we hope to better understand the effects of backgrounds on the event rates on the crystal. The following simulation was designed to study specifically neutron radiation.

5.1   Geometry

The geometry in the simulation involves the osmium crystal mounted atop a copper plate, a lead shield for the purpose of magnetic field shielding, and two aluminum shields[1]. The lead shield and the elements contained within it are housed inside the ADR. There is likely to be some uranium and thorium contamination in the lead shield that will provide some background radiation. However, the results of this paper do not discuss the effects of this radiation.

---

[1]In order to better understand the effects of detector location on the copper plate, the simulation actually includes 5 osmium crystals spread out on the copper plate.
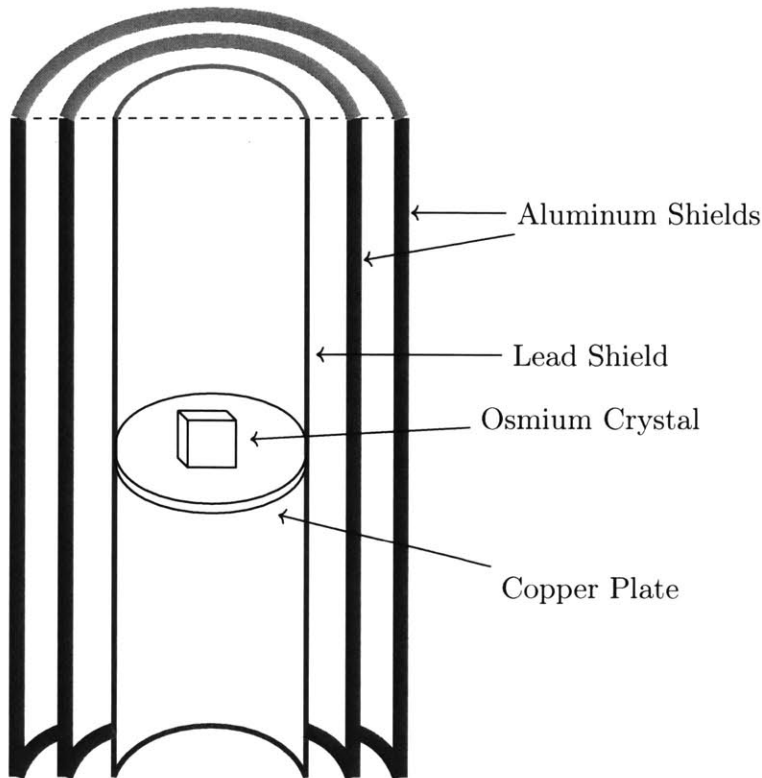
Figure 5-1: A 3D view of the geometry implemented in the simulation. The aluminum radiation shields are each 0.04 inches thick. The lead shield is 1 mm thick.

5.2 Simulation

We run the simulation with an isotropic monoenergetic neutron spectrum. In total, 10 simulations were run with neutron backgrounds, with varying neutron energies[2]. All simulations were run with 5 million neutron events with a source 30 cm away from the detector. As osmium crystals are very difficult to manage, we will first do a test run with zinc crystals when we perform the experiment. This simulation therefore models events on both osmium and zinc crystals.

---

[2]The energies are 0.028 eV, 0.2238 eV, 1.778 eV, 14.125 eV, 112.22 eV, 891.25 eV, 7.079 keV, 56.234 keV, 446.7 keV, 3.548 MeV.
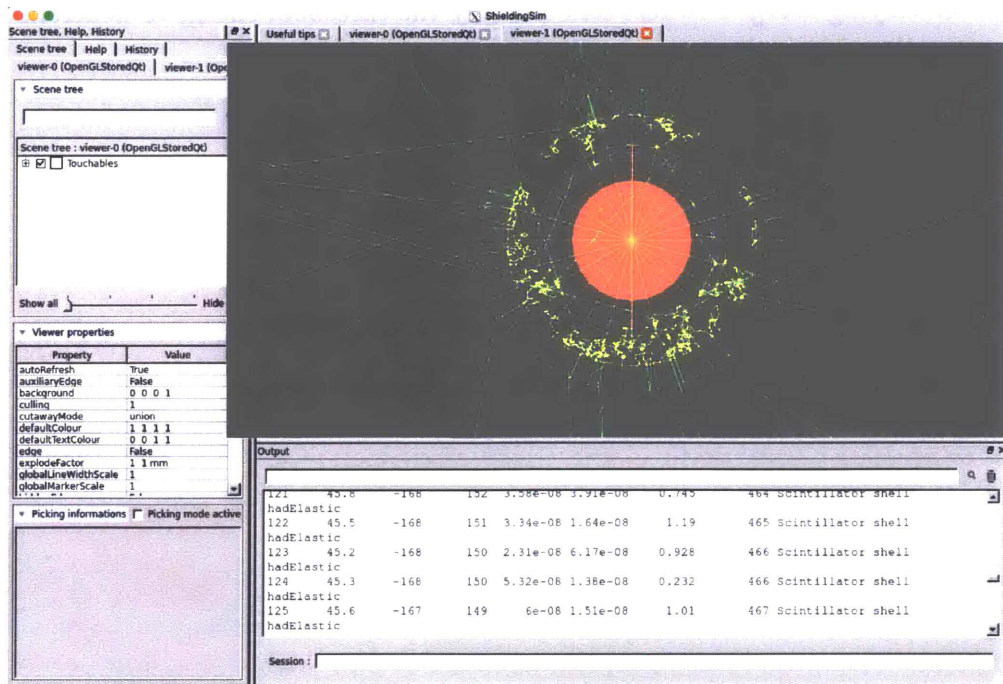
Figure 5-2: A cross sectional view of the simulated geometry in the visualizer. The green lines are neutron trajectories.
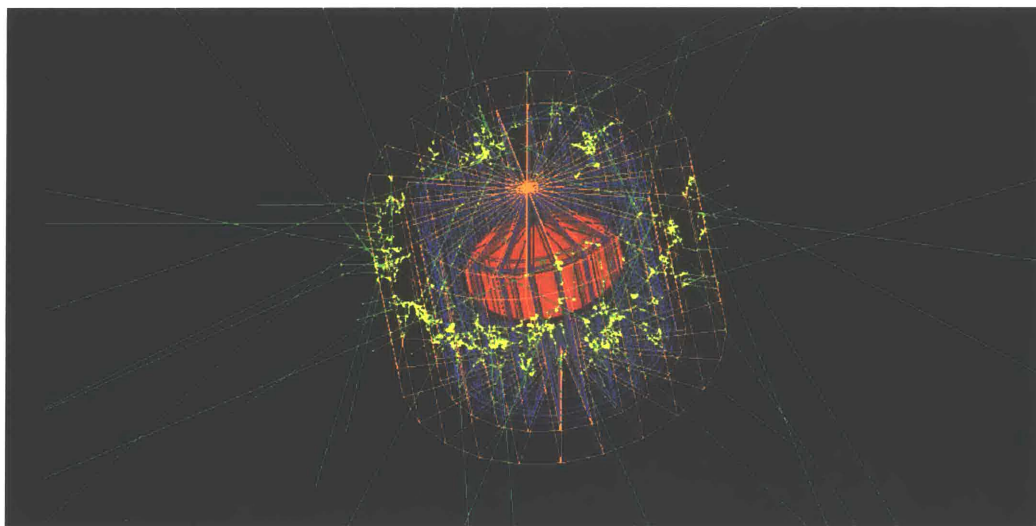
Figure 5-3: A side view of the simulated geometry in the visualizer. The green lines are neutron trajectories.

We predict that higher energy neutrons are the most likely to be detected by this setup. The results from the NCD's will tell us how many high energy neutrons are expected to be present in the system. We run the simulation with monoenergetic neu-

tron sources of varying energies to test and quantify the threshold energy of neutrons that are likely to be detected.

Chapter 6

Neutron Spectra

The results from NCD measurements with the DD source as well as the reactor are shown below. For both the DD source and the reactor, we have the event rates for each layer, and the reconstructed energy spectrum based on the layer data. The reconstructed spectrum from the reactor illuminates what backgrounds we should consider in the simulation and the main experiment. From the simulation and the reconstructed neutron spectrum, we have a rough estimate for the number of neutrons that will be captured by our crystal.

6.1 DD Source Results

DD Source Layer Data
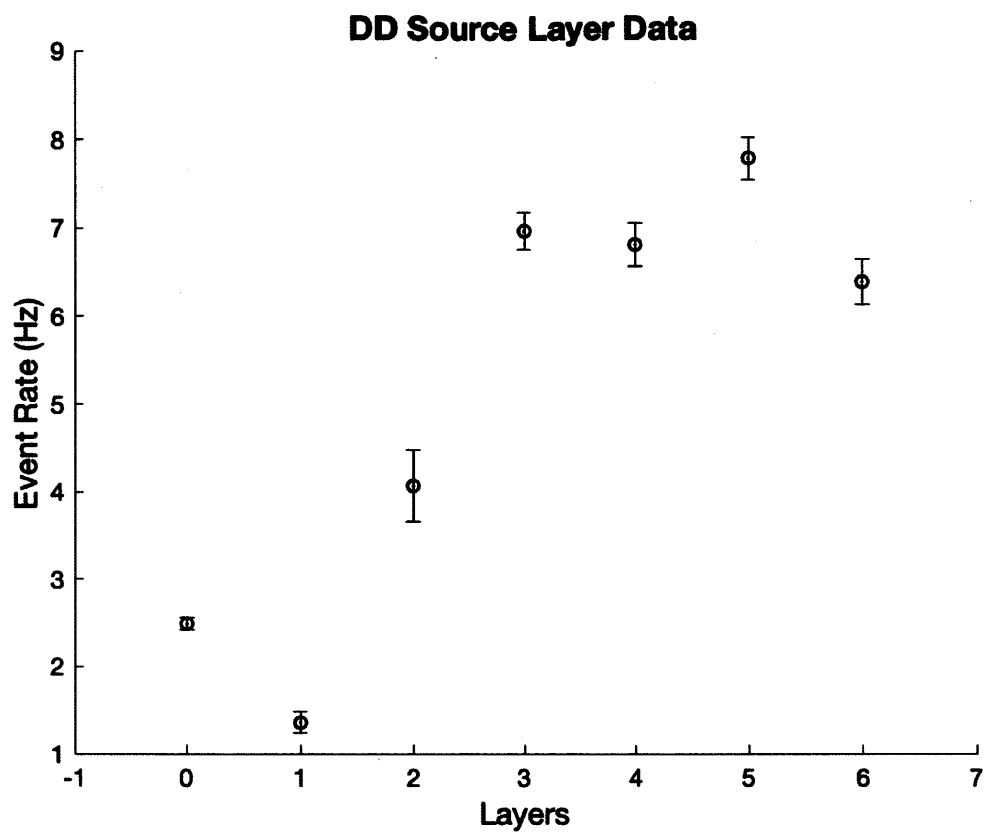
Figure 6-1: Layer data for the DD source.

The DD source produced monoenergetic neutrons at a reasonably high energy (2.2 MeV). Since helium 3 is sensitive to lower energy neutrons, we expected to see the higher event rates with increased shielding that could slow down the neutrons. We see the results are more or less in line with our expectation. We discovered through other radiation monitoring that the neutron production rate fluctuated significantly, possibly accounting for irregularity in the data.
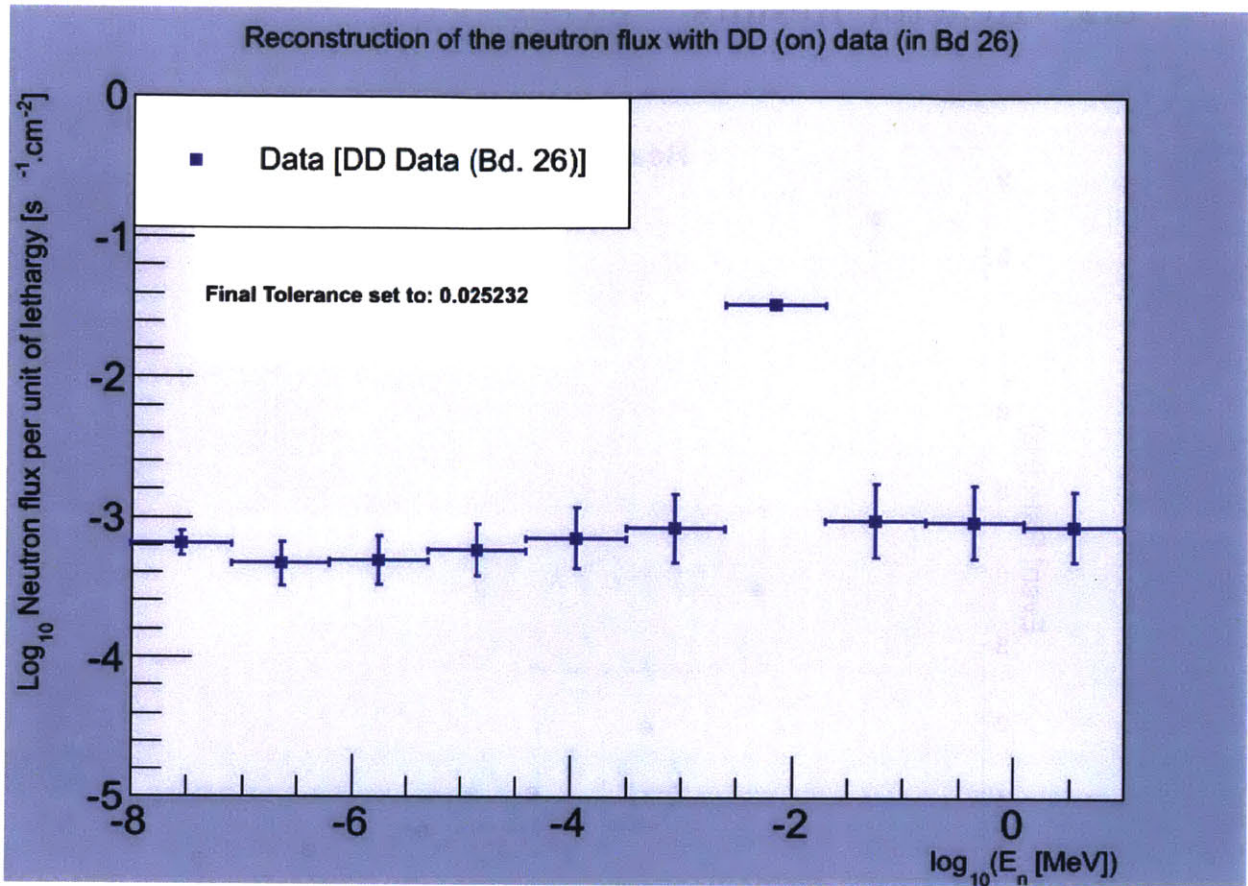
Figure 6-2: Reconstructed neutron spectrum from the DD source. 'Tolerance' refers to a constraint on the likelihood deconvolution that produced this spectrum. The constraint is necessary to prevent the code from choosing extreme possible spectra and then being unable to fit the shape properly, resulting in either a crash or a poor fit. Specifically the tolerance governs the possible shapes the code can choose.

6.2 Reactor Results
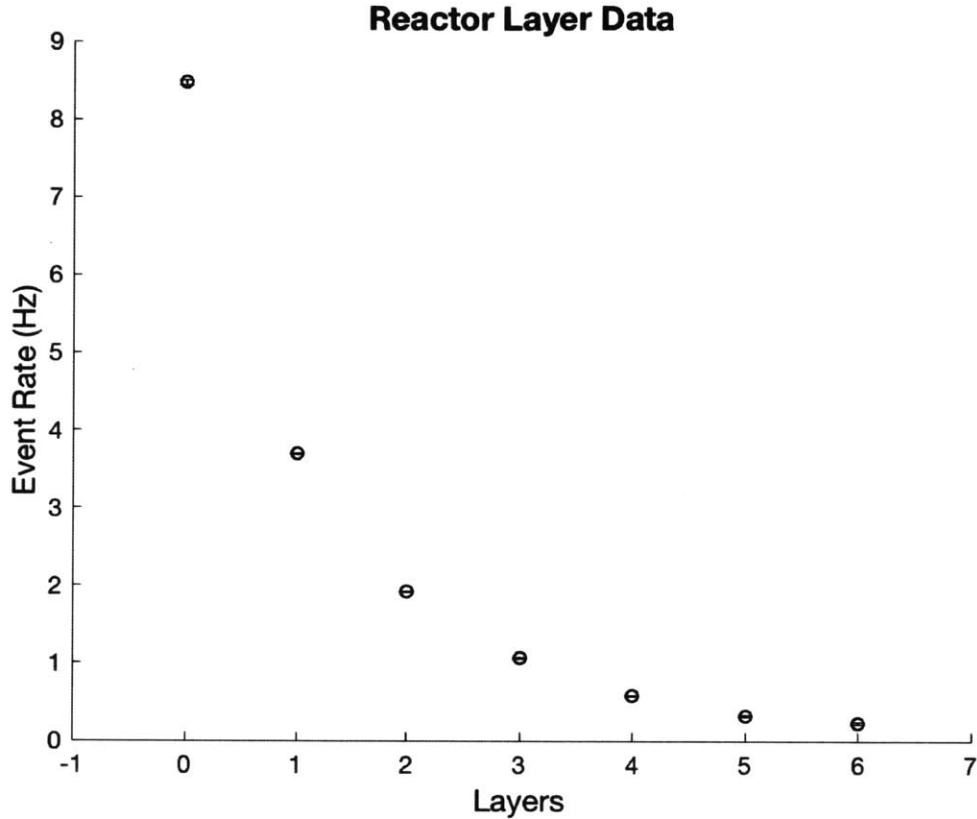
Figure 6-3: Layer data for the reactor.

The NCD/layer system shows very different results for the reactor than for the DD source (as was expected). We see that as the shielding increases, the event rate drops off exponentially. This shows that the reactor produces approximately exponentially fewer high energy neutrons.

We reconstruct a neutron spectrum from the reactor using a likelihood deconvolution. Using the above data, we model the shielding sensitivity to various neutron energy ranges with transfer functions. We then calculate expected event rates for each NCD configuration, assign a likelihood to each proposed spectrum, and then minimize to produce the following spectrum. The uncertainties reported are all statistical.
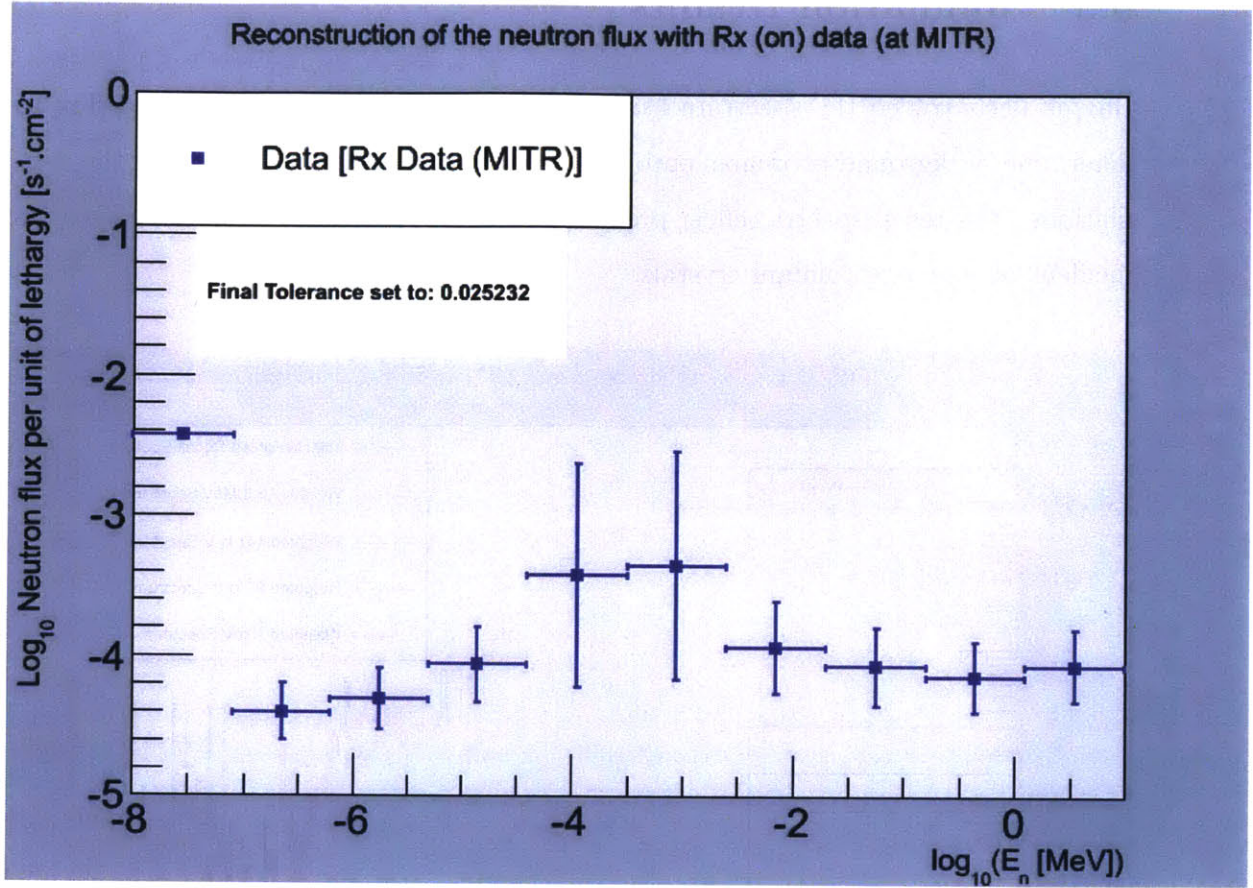
Figure 6-4: Reconstructed neutron spectrum from the reactor.

Below are the steps of the analysis. We calculate expected event rates for different thicknesses from transfer functions,

$$R(x) = \sum_{i=1}^{N_{bin}} \phi(E_i) \int_{E_i}^{E_{i+1}} T(E;x)dE. \qquad (6.1)$$

Here, R is the event rate, $\phi(E)$ is a spectrum, E is the energy, and $T(E;x)$ are the transfer functions for each thickness x. We then calculate a likelihood for each rate by comparing our predictions to our measurements.

$$L[\vec{\phi}(E)] = \exp\left[-\sum_{j=1}^{N_{layers}} \frac{(R_j^{th}[\vec{\phi}(E)] - R_j^{obs})^2}{2\sigma_{R_j^{obs}}^2}\right] \qquad (6.2)$$

43

6.3 Simulation Results

Having deconvolved the spectrum from the data, we now use the measured flux to determine background estimates onto the crystals. Below are the results of the simulations. The recoil spectra reflect predicted neutron event rates for various energies incident on zinc and osmium crystals.
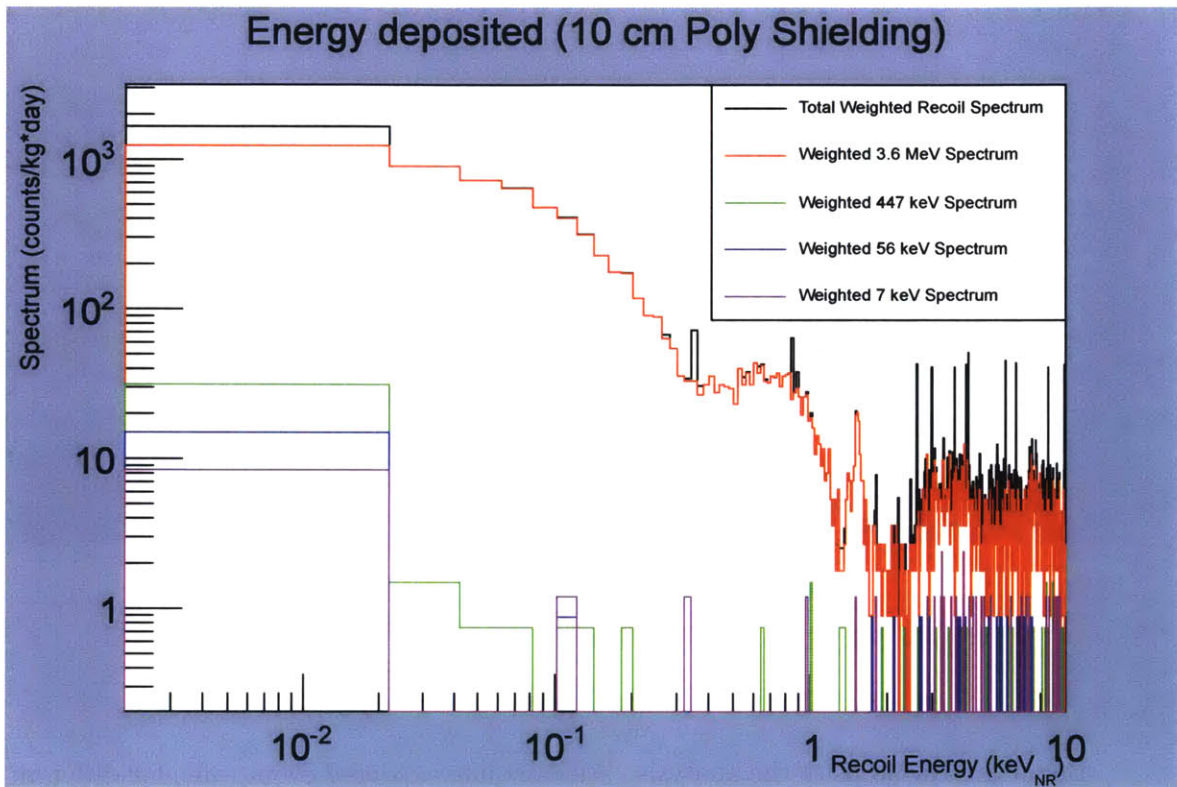
Figure 6-5: Recoil spectrum of neutron backgrounds on osmium crystal.

Table 6.1 shows the total number of events per kilogram of osmium/zinc per day predicted by the simulations when run with the aforementioned neutron energies incident on the crystal in our experimental setup. The table also includes the threshold energies of the neutrons in consideration. The vast majority of these events are due to higher energy neutrons (in this case, 3.6 MeV), which contribute only a small amount of flux to the spectrum from the reactor. The recoil spectrum for the osmium events is shown above in figure 6-5.

Threshold Energy (eV)	events/kg/day (Osm)	events/kg/day (Zn)
100	204 ± 18	137 ± 13
50	242 ± 23	140 ± 13
10	293 ± 27	143 ± 14

Table 6.1: A table showing predicted neutron event rates from the osmium and zinc simulations.

Below is the recoil spectrum of the zinc simulation. We see that the overall event rates are lower for zinc than for osmium but the general shape of the recoil spectrum is the same. The vast majority of events are due to high energy neutrons.
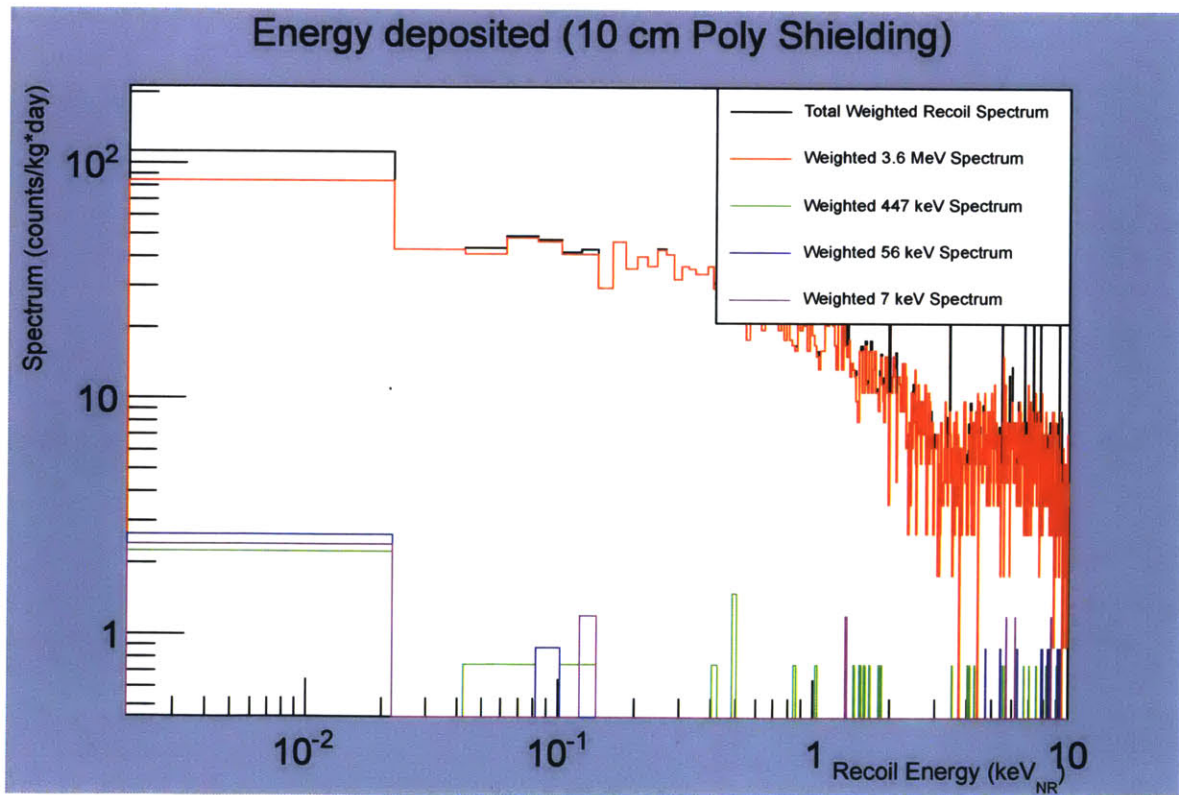
Figure 6-6: Recoil spectrum of neutron backgrounds on zinc crystal.

Chapter 7

Conclusion

In summary, this paper discusses the predicted effects of neutron backgrounds on the Ricochet experiment. The Ricochet experiment proposes the use of coherent neutrino scattering to measure the existence of sterile neutrinos. As coherent neutrino scattering has not yet been observed, it is our goal to first observe this process using the MIT Research Reactor as a neutrino source, and a superconducting metallic crystal array as a detector.

Neutrons are also produced by the reactor. Neutron backgrounds can impart a recoil energy onto the detector, leaving a similar experimental signature as neutrinos. Therefore, it is important that we determine the extent of neutron backgrounds in the system. This paper discusses the calibration of Neutral Current Detectors that are employed for the purpose of neutron detection. The reconstructed neutron spectrum from the reactor that was measured by these detectors was then used to design a Monte Carlo simulation in Geant4. This simulation predicts the total number of neutron events we expect per day with our detector geometry.

The simulation was run with several different monoenergetic neutron sources in the energy range of the spectrum. Two rounds of simulations were run: one with an osmium detector, and one with a zinc detector. Both simulations showed that the vast majority of neutron events that we can expect are due to high energy neutrons, which are scarce in our system.

There is much more work to be done for this experiment. More information is

needed about the number of high energy neutrons produced by the reactor. A more accurate simulation would include information about the shielding around the reactor core as well. Furthermore, gamma backgrounds are also present in the system and can also induce a recoil in the detector. Simulations for different gamma sources should be implemented as well.

Appendix A

ADR Specifications

Cryostat Model 103 Rainier

Small, cylindrical, pulse-tube ADR cryostat

Features:

- Cryomech PT407 Pulse Tube Cooler
- Remote Rotary Valve Motor
- Vibration isolation bellows
- Electronically controlled motorized heat switch
- Quick release flanges on vacuum jackets
- Nickel plated aluminum thermal shields (50 K, 4 K)
- HPD ADR (NIST design)
  - Kevlar Suspension
  - 1 K & 50 mK Stages
- Optimized for versatility and flexibility
  - 4X NW50 ports on top flange
  - 2X NW25 ports on top flange
  - 1X NW63 port on vacuum jacket side
  - 1X Ø6" port on vacuum jacket bottom
- Robust internal construction
- Custom Service Stand (Option)
  - Allows for transport & servicing
  - 30 inches of height adjustment

Specifications:

- Large Experimental Space: 10.2" Diameter X 10" Tall
- Cool down from 300 K to 4 K in 14 hours
- Pulse-tube stage temperatures of 50 K and 2.7 K
- 700 mW cooling power at 4.2 K
- ADR base temperature of 50 mK
- >200 hour no-load regulation at 100 mK
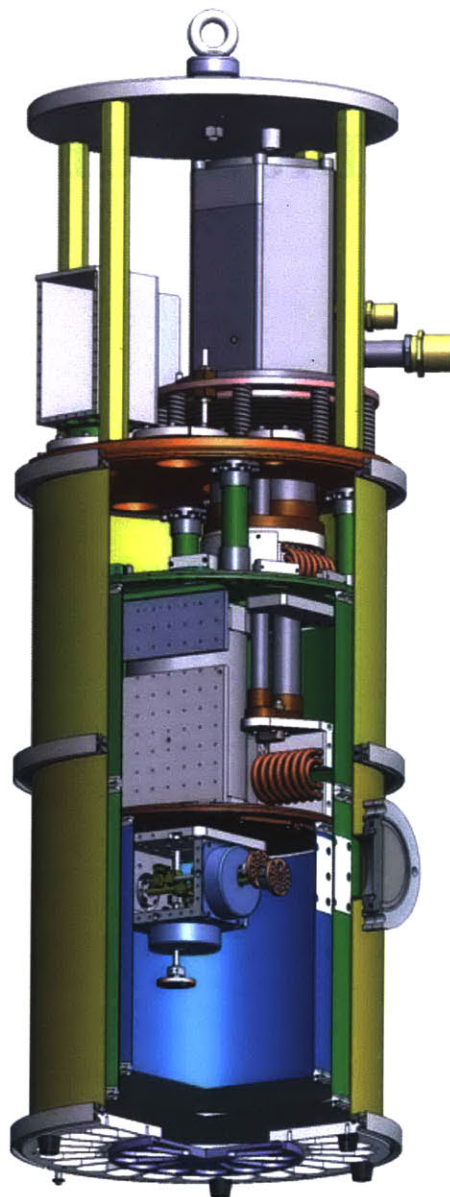
Section view of 103 Rainier ADR cryostat showing pulse-tube head, adiabatic demagnetization refrigerator, high temp superconducting leads for 4 T magnet, thermal shielding.

Model 103 Rainier ADR cryostat showing vacuum jacket, side port, pulse-tube head and anti-vibration bellows.

Model 103 Rainier ADR cryostat showing on the Model 100 Atlas service stand.
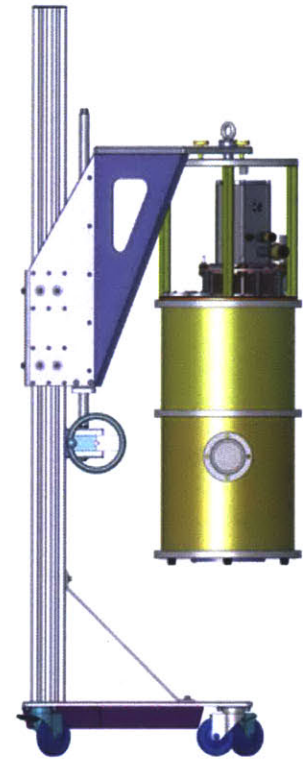
Side view of Model 103 Rainier on the Model 100 Atlas service stand.
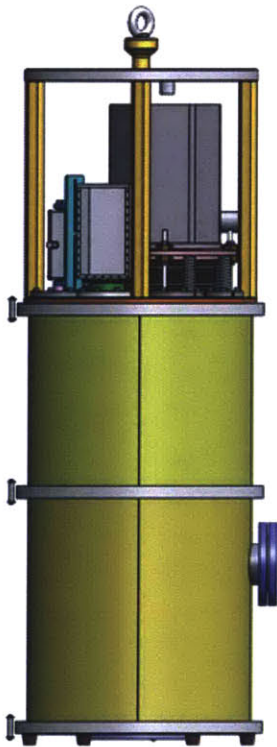
Side view of 103 Rainier ADR cryostat vacuum jacket, side port, pulse-tube head.

Cross-section of 103 Rainier cryostat showing pulse-tube cooler, ADR, thermal links and shields.

Top view of 103 Rainier cryostat showing pulse-tube cooler and feedthrough flanges.

Typical ADR Cooldown
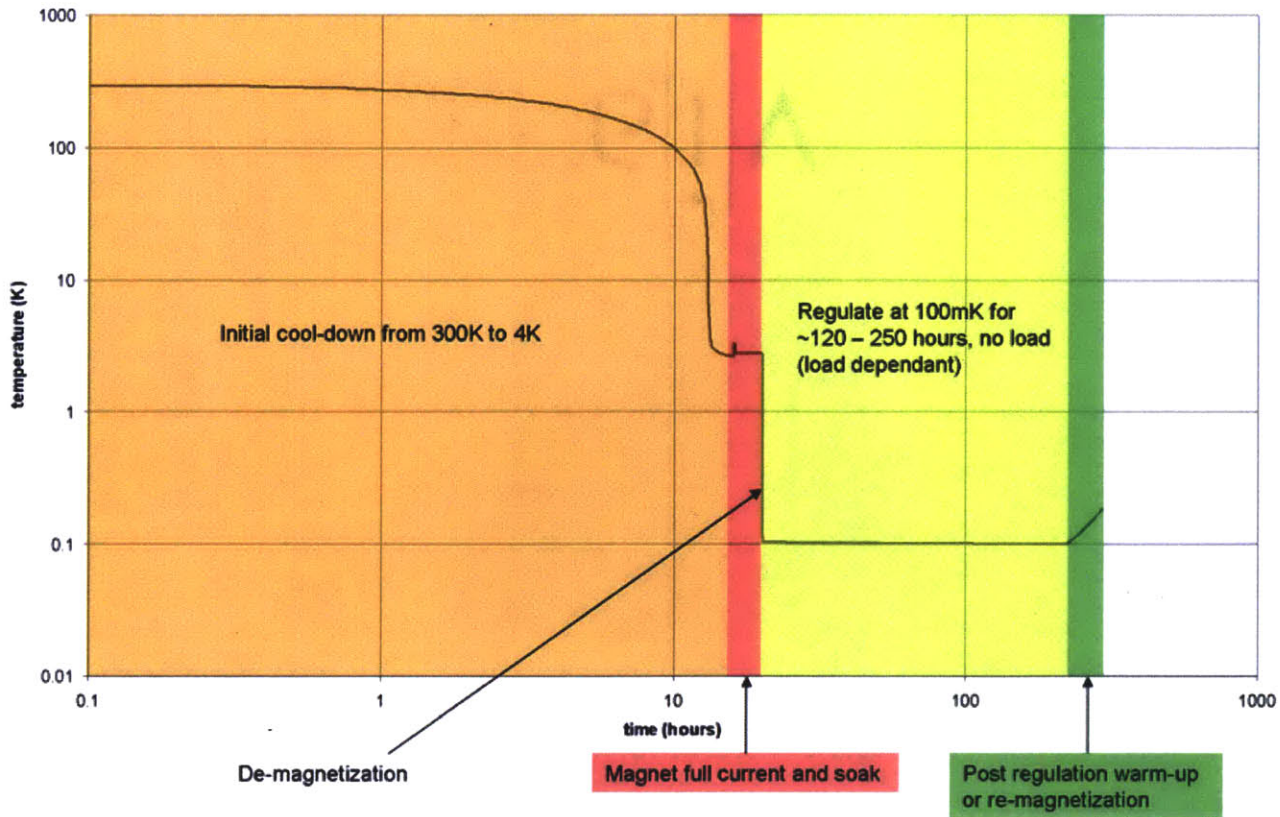
Typical cooling cycle for pulse-tube cooled ADR cryostat.

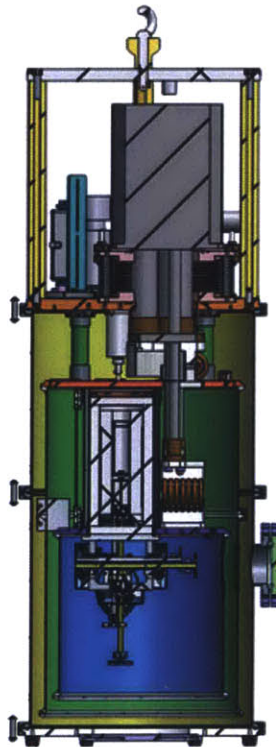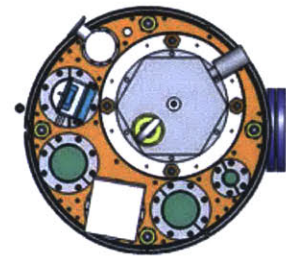| Compare Models					
101 MATTERHORN Wet DR Cryostat	**102 DENALI** Pulse Tube ADR Cryostat	**103 RAINIER** Pulse Tube ADR Cryostat	**104 OLYMPUS** Pulse Tube ADR Cryostat	**105 ANNAPURNA** Dry DR Cryostat	**106 SHASTA** Pulse Tube ADR Cryostat
Vacuum Jacket Size Ø 54 cm X 119 cm Tall	Vacuum Jacket Size 33 cm X 22 cm X 66 cm Tall	Vacuum Jacket Size Ø 35 cm X 69 cm Tall	Vacuum Jacket Size Ø 55 cm X 110 cm Tall	Vacuum Jacket Size Ø 55 cm X 110 cm Tall	Vacuum Jacket Size Ø 44 cm X 65 cm Tall
Experimental Volume Ø 42 cm X 19 cm Tall	Experimental Volume 24 cm X 15 cm X 14 cm Tall	Experimental Volume Ø 26 cm X 25 cm Tall	Experimental Volume Ø 44 cm X 60 cm Tall	Experimental Volume Ø 38 cm X 19 cm Tall	Experimental Volume Ø 34 cm X 21 cm Tall
1st Stage Cooling Power 77 K LN$_2$	1st Stage Cooling Power 25 W @ 55 K	1st Stage Cooling Power 25 W @ 55 K	1st Stage Cooling Power 35 W @ 45 K 40 W @ 45 K	1st Stage Cooling Power 40 W @ 45 K	1st Stage Cooling Power 25 W @ 55 K 35 W @ 45 K 40 W @ 45 K
2nd Stage Cooling Power 4K LHe	2nd Stage Cooling Power 0.7 W @ 4.2 K	2nd Stage Cooling Power 0.7 W @ 4.2 K	2nd Stage Cooling Power 1 W @ 4.2 K 1.5 W @ 4.2 K	2nd Stage Cooling Power 1.5 W @ 4.2 K	2nd Stage Cooling Power 0.7 W @ 4.2 K 1 W @ 4.2 K 1.5 W @ 4.2 K
Lower Stages 1 K LHe Pot .6 K Still .1 K Cold Plate	GGG Cooling Capacity 1.2 J @ 1 K	GGG Cooling Capacity 1.2 J @ 1 K	GGG Cooling Capacity 1.2 J @ 1 K	Lower Stages 1.5 K .6 K Still .1 K Cold Plate	GGG Cooling Capacity 1.2 J @ 1 K
Mixing Chamber Base Temperature 30 mK	ADR Base Temperature < 50 mK	ADR Base Temperature < 50 mK	ADR Base Temperature < 50 mK	Mixing Chamber Base Temperature 30 mK	ADR Base Temperature < 50 mK
Mixing Chamber Cooling Power 150 µW @ 100 mK	FAA Cooling Capacity 118 mJ @ 100 mK	FAA Cooling Capacity 118 mJ @ 100 mK	FAA Cooling Capacity 118 mJ @ 100 mK	Mixing Chamber Cooling Power 200 µW @ 100 mK	FAA Cooling Capacity 118 mJ @ 100 mK

Appendix B

Neutrino Oscillations

Neutrino Oscillations in a Gravitational Field

Elise Newman

MIT Department of Physics, 77 Massachusetts Ave., Cambridge, MA 02139-4307

(Dated: May 1, 2015)

Neutrino flavor oscillations are a phenomenon in quantum mechanics where the probability of measuring a neutrino of a specific lepton flavor oscillates as the neutrino propagates through space. This effect is particularly interesting because it is only possible if the neutrino has mass. Since the Standard Model predicts that the neutrino should be massless, this phenomenon is evidence that the Standard Model is incomplete. In this paper, we will explore the phenomenon and analyze neutrino oscillations in vacuum. Then we will explore neutrino oscillations in the presence of the classical gravitational field of the Earth and Sun, treating the fields as perturbations on the vacuum.

I. INTRODUCTION

Neutrinos are neutral, weakly interacting particles, that are much lighter than electrons. The following discussion on the properties of neutrinos is largely based on Griffiths [3].

In nuclear beta decay, some element A is transformed into a lighter element B via the following process (where e^- is an electron),

$$_Z^N A \longrightarrow _{Z+1}^N B + e^-. \tag{1}$$
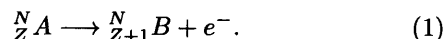
This process should conserve charge and energy. The electron is therefore predicted to have a fixed energy that is determined by the rest masses and momenta of the elements in the reaction. However, experiments at the time showed that the energies of emitted electrons vary significantly. To account for this, in 1930 Pauli proposed the existence of a light, neutral (to preserve charge conservation) particle that could carry away the extra energy. These neutral particles were originally called neutrons but later called neutrinos (which means "little neutral one") due to the discovery of the neutron. Pauli also predicted their mass to be small, but not necessarily zero. Later, it was discovered that there are actually three different types of neutrinos that correspond to the different leptons that produce them in nuclear decay.

Aside from energy and charge, there is a third quantity that must be conserved in decay processes, namely *lepton number*. Leptons are a certain class of spin 1/2 particles that are not subject to strong interactions. There are three different categories of leptons, known as *flavors*, with two particles per flavor: electron and electron neutrino, muon and muon neutrino, and tau and tau neutrino. Each of these leptons also has a corresponding anti-lepton. Leptons are assigned the lepton number $L = +1$ and anti-leptons are assigned $L = -1$. In a decay process, lepton number within flavor must be conserved. (From this it directly follows that overall lepton number must also be conserved.)

These facts are motivated experimentally. For example, it is never observed that a muon decays into an elec-

tron and a photon. Such a process does not violate overall lepton number conservation but it does violate lepton number conservation within flavor. What we actually see is the following decay,

$$\mu \longrightarrow e + \nu_\mu + \bar{\nu}_e, \tag{2}$$
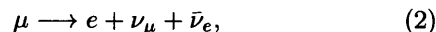
where μ is a muon, ν_μ is a muon neutrino, and $\bar{\nu}_e$ is an electron antineutrino. In this reaction, lepton number within flavor is conserved.

The three neutrino flavors of the Standard Model are considered to be massless in order to follow the Dirac formalism for particles and antiparticles. However, neutrinos have been observed to oscillate between flavors. This can best be explained if there is a mass term in the Lagrangian, which is not diagonal in the flavor basis. In this paper we will explore neutrino oscillations in vacuum as well as in a Newtonian gravitational field.

II. HISTORY OF THE SOLAR NEUTRINO PROBLEM

Before it was known that neutrinos oscillate, there was a long standing puzzle about the measured neutrino flux from our sun. The sun derives the majority of its fuel from hydrogen fusion, given by the following reaction,

$$^1H + {}^1H \longrightarrow {}^2H + e^+ + \nu_e. \tag{3}$$
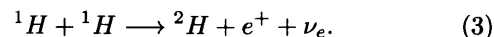
Here, ν_e represents an electron neutrino, e^+ represents a positron, ^1H is a proton and ^2H is deuterium. Based on this reaction, the standard model predicts a certain number of electron neutrinos from the sun to pass through the Earth at any given time. However, experiments throughout the late 1960's to early 2000's have shown that we actually see much less than the predicted value. The history and results of these experiments are discussed extensively in Detmold 2014 [1] and some of the discussion is recreated below.

An experiment conducted by Ray Davis and collaborators at the Brookhaven National Laboratory used

a large tank of perchloroethylene (C_2Cl_4) to detect solar electron neutrinos via Argon decay. Solar electron neutrinos interact with ^{37}Cl, creating Argon and an electron. The Argon was collected over many years to determine that the flux of electron neutrinos from the sun was less than a third of the predicted value.

Many people were skeptical of this result until the SuperKamiokande experiment in Japan confirmed this discrepancy. The SuperKamiokande experiment used a 50,000 ton water tank lined with photomultiplier tubes to measure scattered electrons. When solar electron neutrinos interact with electrons in the water, the momentum imparted on each electron is so great that it gives off *Cherenkov radiation* (results when a charged particle travels faster in a medium than light can). This radiation is detected by the photomultiplier tubes. This experiment recorded about 45% of the predicted number of electron neutrinos.

It had been previously speculated that neutrinos might be oscillating between flavors but it wasn't until 2002 that an experiment confirmed this hypothesis. The experiment was conducted at the Sudbury Neutrino Observatory and it consisted of a large tank of *heavy water*, ($= D_2O$, where $D = {}^2H$), deep in a nickel mine in Canada. Solar neutrinos have an energy of up to roughly 10 MeV, which is much more than the energy required to break apart a deuteron (≈ 2 MeV) into a proton and neutron. By counting the resulting neutrons, it is possible to detect the total number of neutrinos coming from the sun, regardless of their flavor. This experiment measured the flux of solar neutrinos to be about 3 times that of the electron neutrinos measured from the perchloroethylene experiment. This experiment has confirmed that the predicted number of solar neutrinos are passing through the Earth at any given moment. However, only about a third of them are electron neutrinos. Since all neutrinos in the sun are initially electron neutrinos, this shows that the remaining two thirds must have somehow turned into other neutrino flavors, providing evidence for neutrino oscillations.

III. NEUTRINO OSCILLATIONS IN VACUUM

Neutrino oscillations result from a mass term in the Lagrangian that is not diagonal in the flavor basis. This means that every neutrino flavor is a superposition of mass eigenstates; or conversely (since the mass eigenstates are the same as the energy eigenstates), every neutrino energy eigenstate is a superposition of neutrino flavor states. To describe neutrino oscillations formally, we therefore define two bases: the mass basis $\{|\nu_1\rangle, |\nu_2\rangle\}$, and the flavor basis $\{|\nu_e\rangle, |\nu_\mu\rangle\}$. These bases are related by the following transformation (for simplicity, we assume a two state system with just electron and muon neutrinos. It is simple to extend the following analysis to the three state system with bases $\{|\nu_1\rangle, |\nu_2\rangle, |\nu_3\rangle\}$ and $\{|\nu_e\rangle, |\nu_\mu\rangle, |\nu_\tau\rangle\}$.),

$$\begin{pmatrix} |\nu_e\rangle \\ |\nu_\mu\rangle \end{pmatrix} = \begin{pmatrix} \cos\theta & \sin\theta \\ -\sin\theta & \cos\theta \end{pmatrix} \begin{pmatrix} |\nu_1\rangle \\ |\nu_2\rangle \end{pmatrix}. \quad (4)$$

Here, θ is a mixing parameter that controls the coupling of the two bases. The relativistic energy is defined by the rest mass and momentum of the neutrino, yielding $E_j = \sqrt{p^2c^2 + m_j^2c^4}$. For small mass the energy simplifies to $E_j \approx pc + \frac{m_j^2c^3}{2p}$ and we have the energy eigenstates defined by the following Hamiltonian,

$$H_0 = pc\boldsymbol{I} + \begin{pmatrix} m_1^2c^3/2p & 0 \\ 0 & m_2^2c^3/2p \end{pmatrix}. \quad (5)$$

To see why this translates into neutrino oscillation, we will look at an example. Say we have a state that is initially an electron neutrino produced by nuclear fusion in the sun. Written in the mass basis, this electron neutrino is,

$$|\nu_e(0)\rangle = \cos\theta |\nu_1\rangle + \sin\theta |\nu_2\rangle. \quad (6)$$

To describe a mass eigenstate as it propagates from the sun to Earth, we can assume plane wave propagation $\langle z|\nu_j\rangle = e^{i(pz - E_j t)/\hbar}$. We can describe this as a one dimensional system because the only relevant dimension here is the distance between the Earth and sun. It would be more realistic to do the analysis with wave packets instead of plane waves. However, the case we are interested in involves a wave packet that is much wider than the DeBroglie wavelength (h/p), so it is reasonable to approximate the wave functions as plane waves. This approximation is justified because we assume low uncertainty in momentum ($\frac{\Delta p}{p} \ll 1$). This leads to a high uncertainty in position ($\frac{\Delta x}{x} \gg 1$), showing that the wave packet is delocalized over the deBroglie wavelength (which is small because the momentum of these neutrinos is very large). However, since the wave packet is much narrower than the distance over which the neutrino travels, it is still reasonable to discuss the traveling neutrino as a wave packet even though we have written it as a plane wave.

One important note is that this analysis assumes propagation in vacuum. In reality, these electron neutrinos need to travel through a plasma of highly varying electron density as they propagate from the center of the sun to the edge of the sun. This plays a large role in the solar neutrino problem and will be discussed later in Section 4. The following shows the vacuum wave function of the initial electron neutrino after time t and distance z away from the source,

$$|\psi(z,t)\rangle = e^{-i\phi(z,t)}\left(e^{-i\frac{m_1^2 c^3 t}{2p\hbar}}\cos\theta\,|\nu_1\rangle + e^{-i\frac{m_2^2 c^3 t}{2p\hbar}}\sin\theta\,|\nu_2\rangle\right).$$
(7)

The phase factor $\phi(z,t)$ is equal to $\frac{pc}{\hbar}(t - z/c)$ and is common to both mass eigenstates, so it does not affect the probability distribution. The group velocity of the wave packet is c to very high accuracy. Therefore, a neutrino will travel a distance L in roughly L/c, and so we can replace t with L/c and pc with E. Upon making these substitutions the phase becomes one and the final wave function as a function of distance L from the source is,

$$|\psi(L)\rangle = \left(e^{-i\frac{m_1^2 c^3 L}{2E\hbar}}\cos\theta\,|\nu_1\rangle + e^{-i\frac{m_2^2 c^3 L}{2E\hbar}}\sin\theta\,|\nu_2\rangle\right).$$
(8)

To show that neutrinos oscillate between flavors, we compute the probability of measuring a muon neutrino given this initially electron neutrino state. The probability is the square of the overlap of a muon neutrino state with the wave function, $|\langle\psi(L)|\nu_\mu\rangle|^2$,

$$P_{\nu_e}(L) = \sin^2(2\theta)\sin^2\left(\frac{c^3\Delta m^2 L}{4\hbar E}\right),$$
(9)

where $\Delta m^2 = m_1^2 - m_2^2$, and E is the neutrino energy. We see that the probability of measuring a muon neutrino oscillates as the state propagates through space. The probability is maximized when $\sin^2\left(\frac{c^3\Delta m^2 L}{4\hbar E}\right)$ is one, yielding a characteristic oscillation length of $L_{osc} = \frac{4\pi\hbar E}{c^3\Delta m^2}$. We see that both the mixing angle θ and the mass difference must be nonzero. If θ were zero, every mass eigenstate would correspond to a specific neutrino flavor and we would not observe oscillation (the amplitude of oscillation, $\sin^2 2\theta$, would be zero). Likewise, if the neutrinos were massless, we would not see oscillation because the frequency of oscillation would be zero. This shows explicitly the necessity of a massive neutrino.

IV. NEUTRINO OSCILLATIONS IN A GRAVITATIONAL FIELD

Now that we have mathematical framework for describing neutrino oscillations, let us analyze them in a non-vacuum medium. The standard non-vacuum medium used in analyzing neutrino oscillations is lepton-dense matter. Neutrinos interact with very few potentials so this is one of the few effects we can observe. Realistically, the only lepton dense matter we see is electron dense matter [6], as is seen in the sun. The electron density effectively scales the phase in the wave packet by the index of refraction of the medium, $e^{ipx} \longrightarrow e^{ipnx}$. The index of refraction in this case depends on the number density of electrons N,

the momentum of the neutrinos p, and the scattering amplitude $f(0)$, yielding $n = 1 + \frac{2\pi N}{p^2}f(0)$ [2].

This modified phase factor changes the oscillation length of the neutrinos, thus altering the period of oscillation. This effect is known as the MSW effect (because it was explained by Mikheyev, Smirnov, and Wolfenstein in 1978-1986 [2]). The derivation and consequences of this will not be shown here but is discussed in Boehm/Vogel [2].

Once the neutrinos escape the sun, the medium through which they travel is somewhat less dynamic, but still potentially interesting. Let us see what effect gravitational fields have on neutrino oscillations. Neutrinos that propagate from the sun to Earth are subject to the gravitational fields of many bodies. However, these bodies are extremely far away and have a negligible effect. We will just consider the fields of the Earth and Sun. Since gravity is a weak force and neutrinos are extremely small, we expect to be able to treat the gravitational fields as perturbations on the vacuum Hamiltonian. Considering Newtonian gravity, the perturbation takes the following form,

$$\delta H = -\frac{GM_\odot\hat{m}}{r} + \frac{GM_\oplus\hat{m}}{d-r},$$
(10)

where G is the gravitational constant, $M_\odot$ is the mass of the sun, r is the distance of the neutrino from the sun, $M_\oplus$ is the mass of the Earth, and d is the distance between the Earth and Sun. We have defined the mass operator $\hat{m}$ here which has the mass basis as its eigenstates and eigenvalues $\{m_1, m_2\}$. We may use this perturbation to calculate the first order energy shifts and the new wave function. The matrix elements of the perturbation can be found by finding the expectation value of δH with respect to the mass eigenstates,

$$\delta H = \begin{pmatrix} \langle\nu_1|\,\delta H\,|\nu_1\rangle & \langle\nu_1|\,\delta H\,|\nu_2\rangle \\ \langle\nu_2|\,\delta H\,|\nu_1\rangle & \langle\nu_2|\,\delta H\,|\nu_2\rangle \end{pmatrix}.$$
(11)

Using first order time independent perturbation theory, we can compute the shift in wave function. We start with the general formula,

$$|\delta\nu\rangle = \sum_{\nu_i\neq\nu_j}|\nu_i\rangle\frac{\langle\nu_i|\,\delta H\,|\nu_j\rangle}{E_i - E_j},$$
(12)

which for the two state system looks like,

$$|\delta n\rangle = |\nu_1\rangle\frac{|\langle\nu_1|\,\delta H\,|\nu_2\rangle|}{\frac{-\Delta m^2 c^3}{2p}}.$$
(13)

Actually computing these matrix elements is quite messy so we use an original Mathematica script for this

problem. Recent data from SNO and SuperKamiokande estimate θ to be 0.59365 radians. They also estimate a value for Δm^2 at roughly $8 \times 10^{-5} eV^2/c^4$. Estimates for an upper bound on neutrino masses vary but recent papers quote an upper bound of roughly $0.3 \ eV/c^2$ [4]. From this we can find reasonable estimates for m_1 and m_2 and use those values for the computation. The Mathematica script for this computation can be found in the Appendix.

Part of the computation involves integrating over the neutrino path (we are still treating this as a one dimensional problem). We assume that the path in question is the trajectory from the surface of the sun to the surface of Earth.

If we compute the unperturbed energies, we see that they are nearly identical. This causes problems if we try to use non-degenerate perturbation theory. We see that the off-diagonal matrix elements are of order 10^{-22} Joules while the difference in unperturbed energies is of order 10^{-31} Joules, causing the modification to the wave function to be much too large (the unperturbed energies are of order 10^{-12} while the shift in wave function would be of order 10^{+9}). Therefore we must use degenerate perturbation theory. We find the energy shifts due to the perturbation by diagonalizing δH.

The computed eigenvalues appear to have an imaginary part but the imaginary parts are so small in comparison with the real part that they can be regarded as numerical error. The energy shifts we observe are of order 10^{-16} Joules, which is 4 orders of magnitude smaller than the unperturbed energy eigenvalues (called E1 and E2 in the Mathematica script). The best detectors can currently detect neutrinos with energies of tens of keV at the lowest [6]. Since the energy shifts due to gravity are of order 1 keV, the effects of Newtonian gravity on neutrino oscillations are not observable. We expected the effect of gravity to be extremely small because it is very weak and neutrinos are nearly massless, and we see that the results of this computation are consistent with that prediction.

A further possible computation would be to look at the interference of a neutrino in vacuum with a neutrino in a Newtonian gravitational field. A similar computation is done in Sakurai [5] for neutrons in a gravitational field. Interestingly, a phase shift due to gravity was observed for neutrons in 1975 by Colella, Overhauler, and Werner [5]. Given that neutrinos are much lighter than neutrons, we might wonder if the interference for neutrinos would also be observable.

V. CONCLUSION

We have seen that neutrino oscillations are necessary to explain the Solar Neutrino Problem. We have also seen that neutrino oscillations result from the fact that the flavor basis is not diagonal in the energy basis. Since this analysis relies on a nonzero Δm^2, this has as a direct consequence the fact that there must be at least one massive neutrino. If we expand from the two state system to the three state system, there will be a Δm^2 term in the probability of measuring any neutrino flavor given any initial state. From this we can extrapolate that all neutrino flavors must have mass. This has shown that the Standard Model of particle physics is incomplete.

The question of gravitational coupling to neutrino energy is interesting because gravity is one of the few potentials that a neutrino can interact with. As we saw in section 4, lepton dense matter can also affect neutrino oscillation. However, since neutrinos are both neutral and weakly interacting, the MSW effect and coupling to gravity are the only two dynamical effects we could possibly observe. As we saw from the computation in section 4, the effects of gravity are not even observable. This shows how incredibly difficult it is to observe neutrino behavior, which is partly what makes neutrinos and neutrino oscillations so interesting.

[1] William Detmold, *8.05 Notes on Neutrino Oscillations.* Massachusetts Institute of Technology, 2014.

[2] Felix Boehm, Petr Vogel, *Physics of Massive Neutrinos, second edition.* Cambridge University Press, 1992.

[3] David Griffiths, *Introduction to Elementary Particles.* John Wiley & Sons, Inc. 1987.

[4] Naoyuki Haba, Ryo Takahashi, *Constraints on Neutrino Mass Ordering and Degeneracy from Planck and Neutrino-Less Double Beta Decay.* Acta Physica Polonica, 2014.

[5] J. J. Sakurai *Modern Quantum Mechanics* Addison-Wesley Publishing Company, 1994.

[6] Conversation with Prof. Joseph Formaggio

Bibliography

[1] K. N. Abazajian et al. Light Sterile Neutrinos: A White Paper. 2012.

[2] Sea Agostinelli, John Allison, K al Amako, J Apostolakis, H Araujo, P Arce, M Asai, D Axen, S Banerjee, G Barrand, et al. Geant4?a simulation toolkit. *Nuclear instruments and methods in physics research section A: Accelerators, Spectrometers, Detectors and Associated Equipment*, 506(3):250–303, 2003.

[3] John F. Amsbaugh et al. An Array of low-background He-3 proportional counters for the Sudbury neutrino observatory. *Nucl. Instrum. Meth.*, A579:1054–1080, 2007.

[4] A. J. Anderson, J. Conrad, E. Figueroa-Feliciano, J. A. Formaggio, J. Spitz, and M. Pyle. Coherent neutrino scattering with cryogenic semiconductor detectors. In *2012 Electroweak Interactions and Unified Theories*, page 425, 2012.

[5] A. J. Anderson, J. M. Conrad, E. Figueroa-Feliciano, K. Scholberg, and J. Spitz. Coherent Neutrino Scattering in Dark Matter Detectors. *Phys. Rev.*, D84:013008, 2011.

[6] Felix Boehm and Peter Vogel. *Physics of Massive Neutrinos*. Cambridge University Press, second edition, 1992.

[7] David Carpenter, Gordon Kohse, and Lin-wen Hu. *MITR User's Guide*, 2012.

[8] Joseph A. Formaggio, E. Figueroa-Feliciano, and A. J. Anderson. Sterile Neutrinos, Coherent Scattering and Oscillometry Measurements with Low-temperature Bolometers. *Phys. Rev.*, D85:013009, 2012.

[9] Daniel Z. Freedman, David N. Schramm, and David L. Tubbs. The Weak Neutral Current and Its Effects in Stellar Collapse. *Ann. Rev. Nucl. Part. Sci.*, 27:167–207, 1977.

[10] David Griffiths. *Introduction to Elementary Particles*. WILEY-VCH, second edition, 2008.

[11] Páll Theodórsson. *Measurement of Weak Radioactivity*. World Scientific Publishing Co., 1996.